Quaternary Science Reviews 321 (2023) 108383

Contents lists available at ScienceDirect

Quaternary Science Reviews

journal homepage: www.elsevier.com/locate/quascirev

3D morphometry of De Geer Moraines and Crevasse-Squeeze Ridges: Differentiating between pushing and squeezing mechanisms from remotely sensed data

Gwyneth E. Rivers [a,*], Robert D. Storrar [a], Andrew H. Jones [a], Antti E.K. Ojala [b]

[a] Department of the Natural and Built Environment, Sheffield Hallam University, UK
[b] Department of Geography and Geology, University of Turku, Finland

ARTICLE INFO

Handling editor: C. O'Cofaigh

Keywords:
Geomorphology
3D-morphometry
GIS
Remote-sensing
De Geer Moraine
Crevasse-Squeeze Ridge

ABSTRACT

De Geer Moraines (DGM) and Crevasse-Squeeze Ridges (CSR) are important landforms that can provide useful insights regarding palaeo-glacial processes. Specifically, these landforms can provide information concerning ice-marginal dynamics, and/or subglacial processes, depending on the context in which they are formed. The extraction of 3D morphometric data from these ridges can help to elucidate their formational processes, and potentially enable landform differentiation. We develop a new Python-based ArcGIS toolbox that can automatically extract 3D morphometric data from large sample sets of linear features. The morphometry toolbox may be applied to a wide range of research disciplines that are concerned with quantifying the morphometry of any elongated landforms. This is particularly useful for DGM and CSR studies, where visual similarities can result in confusion over landform type and/or formation. Here we present a case study from southwest Finland and the Northwest Territories, Canada, whereby high-resolution 3D morphometric data is used to analyse and classify DGMs and CSRs. The results reveal key differences in morphometric properties between the landforms which enables a quantified foundation by which to differentiate them. The studied CSRs are found to be higher, wider, steeper, more symmetrical, less sinuous and more voluminous than the studied prominent DGM. In contrast, a tendency for cross-sectional asymmetry in DGM supports an origin by ice-marginal pushing, rather than basal squeeze-up into crevasses. This is further supported by CSRs being less sinuous than DGM due to them being constrained to the dimensions and planform of the (relatively straight) host crevasses, whereas DGM follow a more sinuous path related to the ice margin shape. Future work should include sedimentological and geophysical studies to constrain DGM internal architecture and formation processes. The results may then be used to validate the application of DGM for detailed ice marginal reconstructions.

1. Introduction

De Geer Moraines (DGMs) are narrow, elongate ridges that are orientated transverse to former ice flow. These ridges can extend up to several km in length with heights that range from sediment traces of a few centimetres up to 10 m. Widths are typically <50 m, however, they can extend up to 100s of metres wide (Borgstrom, 1979; Finlayson et al., 2007; Golledge and Phillips, 2008; Larsen et al., 1991; Ojala et al., 2015).

Crevasse-Squeeze Ridges (CSRs) are deposits formed within crevasses in glacial ice, often preserving the spatial pattern of crevassing (Benn and Evans, 2010). CSRs can provide important information concerning palaeo-ice sheet subglacial processes, which can be used to assist with understanding contemporary ice sheet behaviour (Evans et al., 2016; Rea and Evans, 2011) (Fig. 3A & B).

Morphometry deals with the measurement of form and is an integral aspect of geomorphological studies (King, 1982; Evans, 2012; Pike et al., 2009). Morphometry enables a deeper understanding of form and process to be developed, and allows for the differentiation of different landform types, which can facilitate the development of classification criteria, landscape evolution models and process-form models (Valters, 2016; Li, 2020). This is particularly pertinent to landforms that possess similar morphology, which often leads to uncertainty of identification and interpretation among researchers, thereby resulting in unclear

* Corresponding author.
E-mail address: Gwyneth.Rivers@student.shu.ac.uk (G.E. Rivers).

https://doi.org/10.1016/j.quascirev.2023.108383
Received 3 July 2023; Received in revised form 17 October 2023; Accepted 26 October 2023
Available online 9 November 2023

implications.

DGMs and CSRs are landforms with generally similar dimensions, they both occur in swarms, are broadly oriented transverse to ice-flow and may therefore be difficult to qualitatively distinguish and correctly classify. Their differing formation processes/environments and different glacial dynamics mean it is important to distinguish between them and use them appropriately for reconstructing past retreat/behaviour/conditions of former ice sheets. A key example of this is the ambiguity of whether DGMs are ice marginal or crevasse infill deposits, and whether they are formed annually or sub-annually (Beaudry and Prichonnet, 1991 & 1995; Blake, 2000; De Geer, 1940; Hoppe, 1959; 1957 & 1959; Streuff et al., 2015). An initial step to address this issue is to quantify detailed morphometry of each individual landform at large sample sizes to identify any key differences in form, based on cases where the landform type can be confidently identified/interpreted visually. This will help to develop a more detailed understanding of the formational processes/environment for each landform and enable a more accurate basis by which to differentiate them.

The quantification of feature morphometry requires the accurate measurement of geometric properties. Whilst basic morphometrics (e.g. length, width, and height) of a given landform may be quantified with relative ease, this can become more complex when dealing with large datasets and landforms defined by high spatial variability (Storrar et al., 2015). Furthermore, traditional mapping approaches tend to map along centre-lines of landforms and/or outlines. This provides direct information relating to basic geometries (length, sinuosity, footprint area, orientation), however, further manipulation is required to extract metrics such as along-line, or within-area, elevation, height, asymmetry, and volume. This is particularly pertinent to elongated landscape features such as eskers, DGMs and CSRs, whereby morphometry varies along a feature's length. Such variability might be important for interpreting the origin of a landform, or even understanding varying glacial settings and depositional environment during its formation. In addition, more detailed 3D analysis information may be required if landform type is difficult to establish. This is particularly relevant when attempting to identify morphometrically complex landforms (e.g. Butcher et al., 2016).

A second key challenge of morphometric analysis is the complex integration of appropriate GIS tools. The integration of multiple tools and geoprocessing methods can become time-consuming and characterised by complex workflows. This issue becomes further amplified when dealing with large datasets.

The purpose of this study is to: (1) develop and test a new automated method of extracting terrain 3D morphometric data of elongated landforms at large sample sizes, and (2) acquire 3D morphometric data of DGMs and CSRs to enable their differentiation and to gain insights into their formation processes, including testing whether DGMs are formed by squeezing into basal crevasses or by pushing at ice margins.

To overcome some of the challenges described above concerning morphometric analysis, a new method has been developed in the form of an open-access Python-based ArcGIS toolbox that automatically extracts 3D morphometric data at user-specified segmented transect intervals. This new method has built upon the approaches taken in previous studies (Storrar et al., 2015; Butcher et al., 2016), expanding the range of morphometric data captured and automating the data extraction process to enable larger datasets to be generated with ease.

This paper presents a case study whereby high-resolution 3D morphometric data, obtained through the developed morphometric toolbox, is used as a primary step to classify and differentiate between DGMs and CSRs. The case study demonstrates how the toolbox automatically calculates 3D morphometric data at user-defined segmented-transect intervals, generating a highly detailed morphometric dataset that can be used to perform individual feature assessments and/or wider analyses of spatial distribution. Our aim is to test the effectiveness of the method and to increase our understanding of DGM and CSR morphometry, especially with respect to similarities and differences related to the proposed formation hypotheses. Furthermore, this case study demonstrates how the toolbox can be applied to wider research areas concerning any elongate morphology, whereby a high-resolution 3D morphometric quantification is required.

The ambiguity of DGM and CSR interpretation presents several key implications for reconstructing palaeo-ice marginal environments and raise several research questions for understanding ice sheet behaviour:

- Are DGMs ice marginal formations?
- If DGMs are ice marginal features, are they annual or sub-annual formations?
- Can DGMs be used as an effective ice marginal chronometer?
- Can we accurately differentiate between CSRs and DGMs?

It is clear that DGMs have the potential to act as a powerful indicator for ice marginal spatiotemporal properties, yet there is still much work to do in order to accurately quantify these landforms. As such, this paper will focus on the spatial aspects of DGMs and seek to investigate if it is possible to differentiate between DGMs and CSRs.

2. Formation of De Geer Moraines and Crevasse-Squeeze Ridges

2.1. De Geer Moraines

DGMs are narrow, elongate ridges that are orientated transverse to ice flow. They were first observed in Sweden and described as small, regular frontal moraines by De Geer in 1889 (De Geer, 1940) who interpreted them as annual moraines; these were then later coined 'De Geer moraines' by Hoppe (1959). They can present as linear, concave, or convex in profile, depending on local topographic controls, and have been observed with both symmetrical and asymmetrical geometries, often displaying a steeper distal side (Hoppe, 1959; Golledge & Phillips et al., 2008; Ojala et al., 2015). They typically occur in swarms of successive ridges observed to cover large tracts of terrain. The ridges may cluster within those tracts, exhibiting high parallel conformity, with either regular or irregular arrangements. The low-lying terrain in between the ridges can often be covered by postglacial silt and clay (Fig. 1; Ojala et al., 2015 & 2016). Observations are most common in low-lying terrains, below the highest shoreline of proglacial lakes/seas, where the grounding-line was subaqueous (Hoppe, 1959; Embleton and King, 1968; Linden and Moller, 2005; Ojala et al., 2015 & 2016; Larsen et al., 1991; Bouvier et al., 2015; Finlayson et al., 2007; Lundqvist, 1981), although observations have also been made in mountainous-valley, lacustrine environments (Borgstrom, 1979; Golledge and Phillips, 2008). Due to the modest amplitude and low relief environments in which they reside, preservation potential is variable and heavily influenced by topography and fluvial reworking (Aartolahti, 1972). Furthermore, postglacial sedimentation can create challenges with respect to landform detection.

DGMs have also been referred to as: calving moraines (Frödin, 1916), cross-valley moraines (Embleton and King, 1968; Hoppe, 1959), end moraines (Smith and Hunter, 1989), wash-board moraines (Mawdsley, 1963), minor moraines (Smith, 1982) and transverse eskers (Virkkala, 1963). The variety of descriptions allude to the ambiguity surrounding both the spatial and temporal properties of DGMs which have been heavily disputed since their first description. A review of existing literature indicates two dominant formation hypotheses:

1) A sub-aqueous, ice-marginal process characterised by the advection and push of basal till to the grounding-line during seasonal advances. Upward buoyancy strains on the ice result in calving and thus preserve the deposited till. This depositional theory was proposed by De Geer in 1889 (De Geer, 1940) and there is a large body of subsequent research that support this model (Smith, 1982; Smith and Hunter, 1989; Blake, 2000; Finlayson et al., 2007; Larsen et al., 1991; Linden and Moller, 2005; Borgstrom, 1979; Golledge and Phillips, 2008;

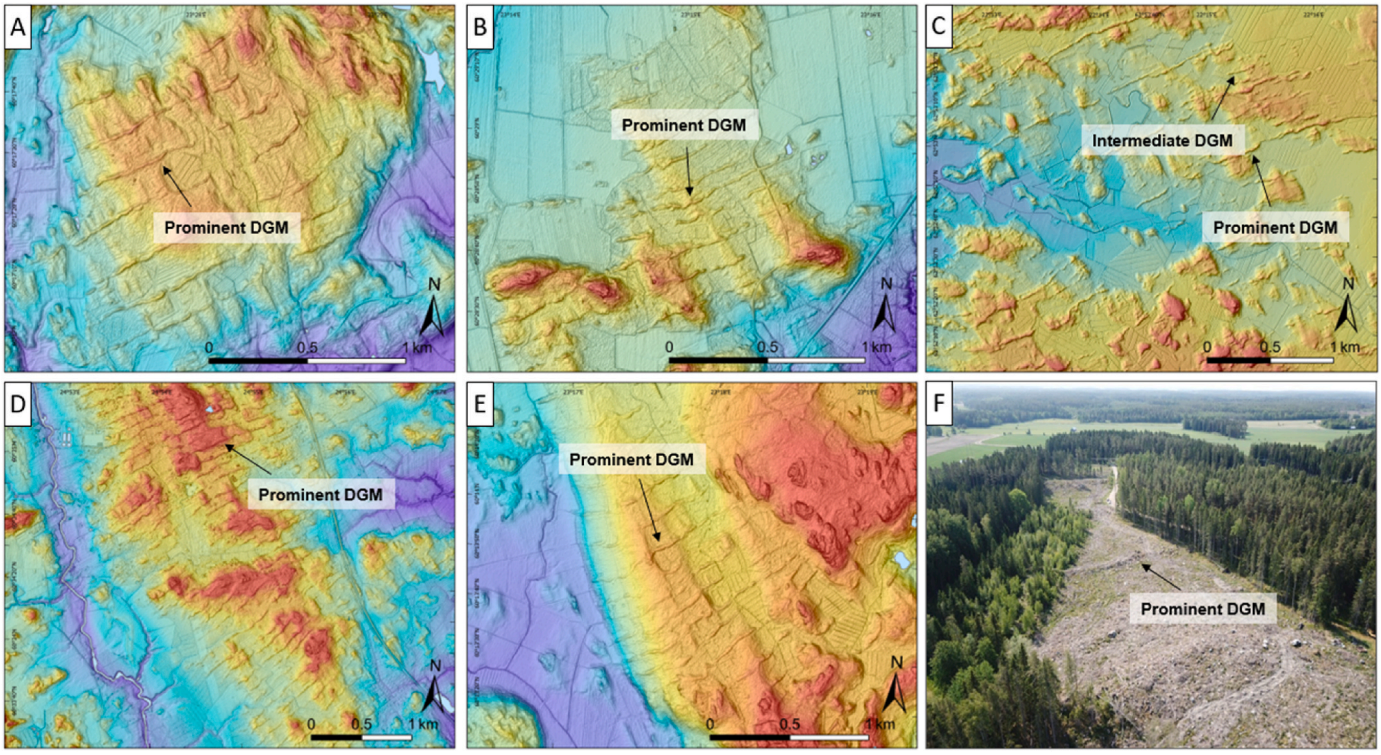

Fig. 1. Digital Elevation Model (DEM) with multi-directional hill shade (MDOW) and oblique aerial drone imagery capturing distinct and regularly spaced De Geer moraine formations situated in SW Finland. Intermediate De Geer moraines can also be seen in image C. A) Torholankulma, Salo; B) Kurimäki, Salo; C) Konnonperä, Isokyrö; D) Palpuro, Hyvinkää; E) Haaro, Perniö and F) Suorsalantie, Mynämäki [DEM source: ®National Land Survey of Finland, LiDAR digital elevation model, 2/2023].

Aartolahti, 1972; Dix and Duck, 2000; Sollid, 1989) (Fig. 2A). In addition to the depositional model, De Geer (1940) also interpreted DGMs as forming annually. Much research has been undertaken to test this hypothesis, comparing ridges to varve chronologies (Hoppe, 1959; Hoppe, 1957; Möller, 1962; Stromberg, 1965), as well as investigating their sedimentological properties (Blake, 2000; Linden and Moller, 2005; Lundqvist, 1981; Hoppe, 1959; Hoppe, 1959). These investigations presented challenges to the annual formation hypothesis, for example, finding additional moraines to the number required by the varve chronologies (Hoppe, 1957; Stromberg, 1965), and suggestions of several annual till layers embedded within a single ridge (Linden and Moller, 2005). De Geer (1940) also suggested that a distinction could be made between smaller, intermediate, ridges, positioned between more prominent, distinct ridges (Fig. 1C). Some authors interpreted these smaller ridges as interannual, with the prominent ridges being annual (Hoppe, 1959; Möller, 1962), however, Stromberg (1965) challenged this idea, emphasising the lack of definitive evidence to suggest that prominent ridges form annually, as well as the difficulties in distinguishing between prominent (annual) and smaller (interannual) ridges due to morphological similarities. Amongst other ideas, these problematic observations led to proposals that the ridges were formed in basal crevasses, therefore possessing no geochronometric value.

2) A sub-glacial process characterised by the squeezing of sediments into basal or full-depth crevasses (Beaudry and Prichonnet, 1991; Beaudry and Prichonnet, 1995; Hoppe, 1959; Mawdsley, 1963; Zilliacus, 1989). This hypothesis suggests that crevasses are formed up-ice of the subaqueous ice margin due to an increase in flow velocity initiated by enhanced basal lubrication. During seasonal variations in hydrology, as meltwater pressure decreases and basal drag increases, the ice sinks into the bed and sediment is squeezed up into basal ice cavities, thus forming 'crevasse-squeeze ridges'. The preservation of these landforms would require the ice to be lifted from the bed and followed by calving. This implies synchronous formation, and therefore suites of landforms do not contain any clear temporal (time-transgressive) characteristics (Fig. 2B).

A secondary variation of this crevasse infill theory is the injection of channelised, sediment-laden meltwater which transports and deposits sediments into basal crevasses, rather than a pressurised up-squeezing of basal sediments, although it is likely that these processes are not exclusive during sediment infilling (Beaudry and Prichonnet, 1991; Beaudry and Prichonnet, 1995; Evans et al., 2022; Sollid, 1989) (Fig. 2C).

Irrespective of the crevasse infilling process, the contrasting formation theories (in a crevasse or at an ice margin/grounding line) warrant further investigation. In this respect, it is useful to consider CSRs, which are definitively formed within crevasses, and which are discussed below.

2.2. *Crevasse-Squeeze Ridges*

Crevasse-Squeeze Ridges (CSRs) are deposits formed within crevasses in glacial ice, often preserving the spatial pattern of crevassing (Benn and Evans, 2010). CSRs can provide important information concerning palaeo-ice sheet processes, at both local and regional scales, such as variations in pressure gradients, subglacial hydrological regimes, strain rates, and fracture patterns and distribution, all of which can be extrapolated to assist with understanding contemporary ice sheet behaviour (Evans et al., 2016; Rea and Evans, 2011).

CSRs are commonly described as straight, narrow, sharp-crested ridges, usually arranged in geometric networks (Fig. 3). Typical morphometrics can be summarized as: height; 1–8 m (although they have been described as sediment traces with heights of only a few cm whilst also extending up to 18 m high) (Benn and Evans, 2010; Ben-Yehoshua, 2017; Kurjanski et al., 2019; Sharp, 1985; Sobota et al., 2016), width; 0.5–2 m, have been observed up to 7 m in terrestrial environments

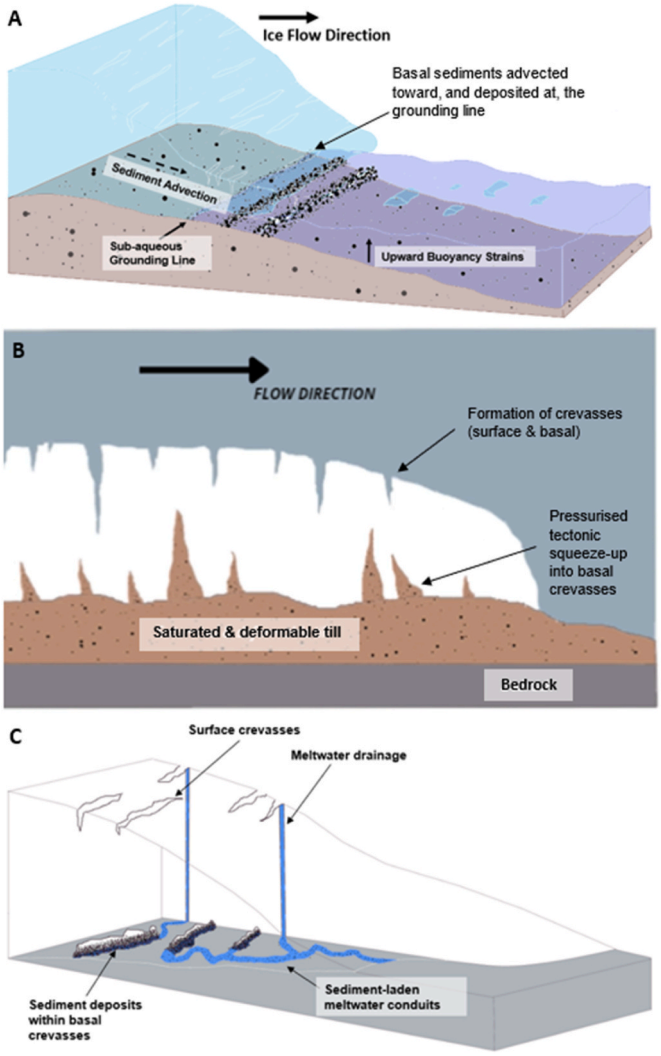

Fig. 2. Schematic diagrams of De Geer moraines formation theories. A) Ice-marginal push/advection' formation theory. A subaqueous ice-marginal process whereby subglacial sediment is advected toward the grounding line and deposited as transverse ridge formations. Formations are preserved due to calving processes; B) Crevasse infill theory of De Geer moraines. Diagram illustrates a pressurised, tectonic squeeze-up of saturated sediments into basal crevasses; C) Channelised meltwater conduit formation theory. Diagram illustrates meltwater drainage via surface crevasses. Sediments are then deposited within basal crevasses behind the ice margin via sediment-laden meltwater conduits.

(Ben-Yehoshua, 2017; Sobota et al., 2016) and up to 270 m in submarine environments (Kurjanski et al., 2019), length; highly variable, often <100 m (Evans et al., 2016; Ó Cofaigh et al., 2010), although have been described up to several hundred meters (Clapperton, 1975; Kurjanski et al., 2019). Slope angles have been observed up to 70–80° (Lovell et al., 2015), however, it should be noted that extent and slope of these ridges are highly dependent on preservation potential, whereby slope decreases with sustained subaerial exposure (Ben-Yehoshua, 2017). Furthermore, many authors have described interstitial ice content as a characteristic of these ridges, therefore preservation is vulnerable to melt-out reworking (Evans and Rea, 1999; Sharp, 1985).

The spatial distribution, size and patterning of CSRs are highly variable due to the various stress patterns produced in different topographic and ice dynamic settings. Some studies describe distinct geometrical ridge networks, with rhombohedral, cross-cutting/intersecting patterns (Lovell et al., 2015; Ottesen and Dowdeswell, 2006 & 2008; Solheim, 1991), others describe patterns of linear ridges orientated transverse to sub-parallel to former ice flow (Clapperton, 1975; Kurjanski et al., 2019; Sharp, 1985), some describe networks as a branched ridge system (Ben-Yehoshua, 2017), and others have described more chaotic-like patterns with attenuated ridges that have no preferred orientation (Lovell et al., 2015).

CSRs have historically been considered diagnostic of, and predominantly related to, surge-type glaciers since these generate extension, and preservation due to stagnation (Benediktsson et al., 2009; Evans and Rea, 1999; Ingólfsson et al., 2016; Ó Cofaigh et al., 2010). However, these features are becoming more commonly observed in palaeo-ice stream settings (Andreassen et al., 2014; Evans et al., 2016; Greenwood et al., 2017; Kurjanski et al., 2019), thereby highlighting that these landforms may provide critical information pertinent to ice stream function and evolution. This is important as ice streams are known to play a major role in reducing ice sheet volume (Bennett, 2003; Stokes and Clark, 2001; Stokes, 2000, 2018). As such, the assessment of CSR patterns and morphometry may provide useful data for reconstructing flow configurations and enabling a deeper understanding of ice stream processes. Moreover, since CSRs are known to form by squeezing into basal crevasses, quantification of their morphometry provides a useful dataset against which to compare DGMs in order to assess the mode of DGM formation (i.e. if they also form by squeezing into crevasses, they should have similar morphometry).

3. Study areas

3.1. De Geer Moraines

DGMs are particularly abundant across south-west Finland, where DGM fields are related to the retreat of the Fennoscandian Ice Sheet (FIS) during the Weichselian deglaciation (e.g. Mäkinen et al., 2007; Ojala, 2016). In this area, the retreat of the FIS during the Late Weichselian and the Early Holocene is well constrained by geomorphology and dating using varved clay chronology, radiocarbon, luminescence, and cosmogenic methods (e.g. Sauramo, 1923; Batchelor et al., 2019; Hughes et al., 2016; Stretch et al., 2006). By the end of the Weichselian, the retreating FIS was divided into several ice lobes (discrete ice streams with intervening 'interlobate' zones) in Finland, which operated time-transgressively and formed the unique Salpausselkä ice-marginal formations during the Younger Dryas (Boulton et al., 1996; Mangerud et al., 2022). The presently studied De Geer moraine ridge fields lie within the southern sector of the Baltic Sea Ice Lobe and mostly up-ice from the First and Second Salpausselkä (Fig. 4). This area contains the classical fields of DGM in SW Finland – the Eura-Lavia, the Mynämäki-Pyhämää and the Halikko-Suomusjärvi De Geer moraine fields (Zilliacus, 1989; Mäkinen et al., 2007; Ojala, 2016) – that present a distinct and rhythmic pattern of ridges, characteristic of DGMs (Fig. 1). Due to the abundance and distinct regularity, this area has been deemed valuable for offering a large sample dataset with which to study morphometry and test spatial properties.

3.2. Crevasse-Squeeze Ridges

The CSRs used in this study are associated with the Great Slave Lake Ice Stream (Margold et al., 2015), located in the interior plains of Northwest Territories, Canada (Fig. 5A). The CSRs in this area are arranged in a linear swarm, spanning a section inside of the ice stream shear margin (Fig. 5B). They exhibit clear geometric networks with evidence of cross-cutting, oblique and contrasting orientations (Fig. 5B), consistent with well-documented observations of CSRs elsewhere (e.g. Evans et al., 2016; Ó Cofaigh et al., 2010; Norris et al., 2018; Ross et al., 2009; Cline et al., 2015; Ankerstjerne et al., 2015). In addition to their diagnostic spatial patterns, their presence at a shear margin, a region of high extensional stress, is also consistent with a crevasse origin. A total of 1159 ridges were identified across an area of 20 km^2.

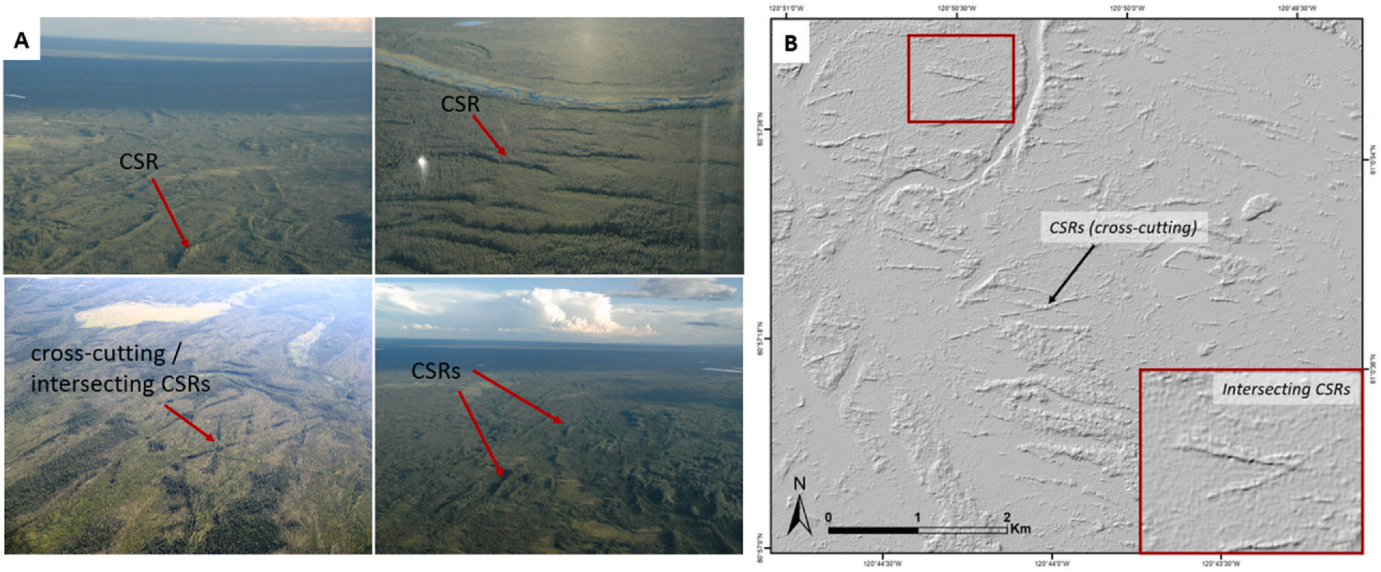

Fig. 3. A) Series of aerial photographs of CSR landforms located in the Northwest Territories, Canada [courtesy of Roger Paulen]. B) Hillshaded DEM showing example CSRs identified across a section of the former Great Slave Lake ice stream, northwest Territories, Canada [DEM source: ArcticDEM – Porter et al., 2018].

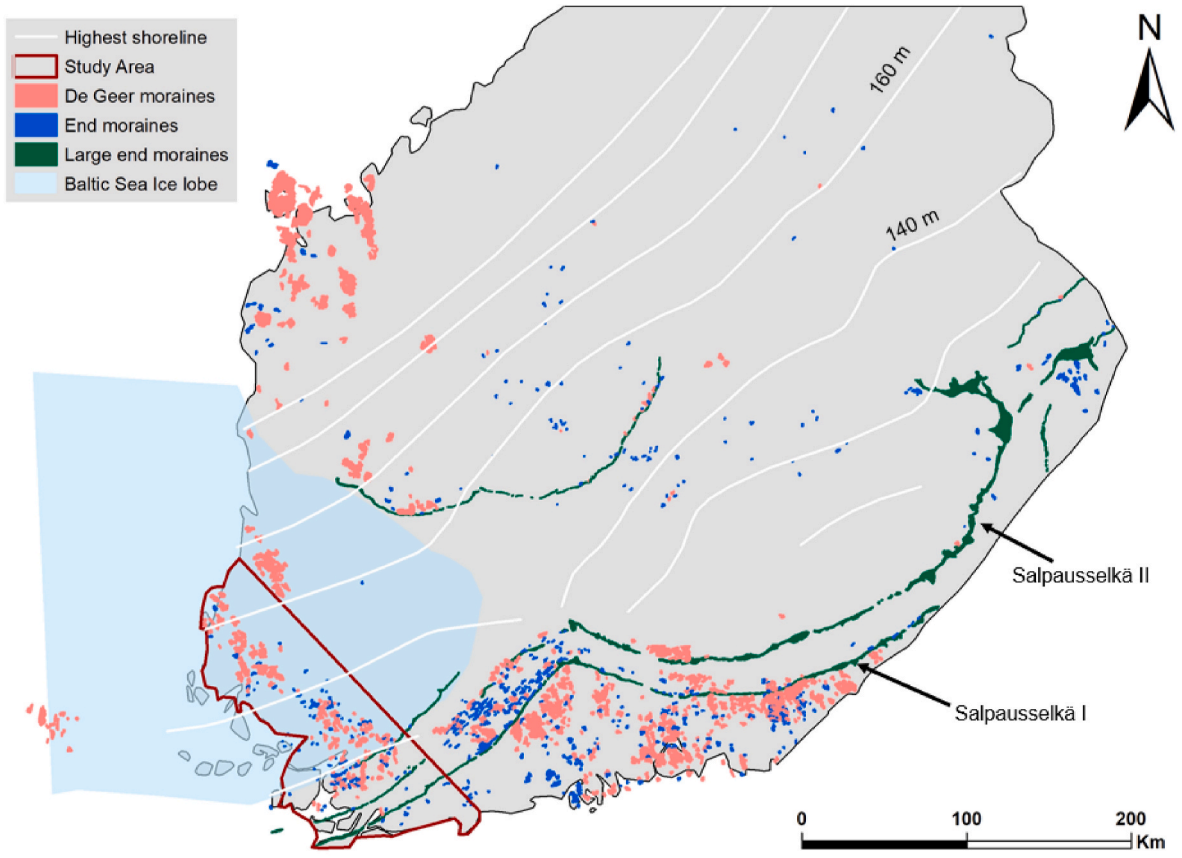

Fig. 4. Study area chosen for DGM data collection located in southwest Finland. The location of De Geer moraine fields has been updated from Ojala (2016) and Baltic Sea Ice Lobe boundary and large end moraines (e.g. Salpausselkä moraines) positions are based on Palmu et al. (2021). The study area encompasses DGMs that are positioned northwest of the second Salpausselkä moraine.

4. Methods

To extract and calculate 3D morphometry for large sample sizes, a Python-coded ArcGIS toolbox was created. The toolbox comprises two tools: (1) a primary '3D Morphometry Tool'; and (2) a secondary 'Average Feature Tool'. Specifically, the primary tool is intended to extract and calculate detailed 3D morphometry, at user-defined, transect-segmented intervals, along the length of a set of target landscape features. The secondary tool is then available to calculate the mean of each transect morphometric per 'parent' feature to provide a whole-

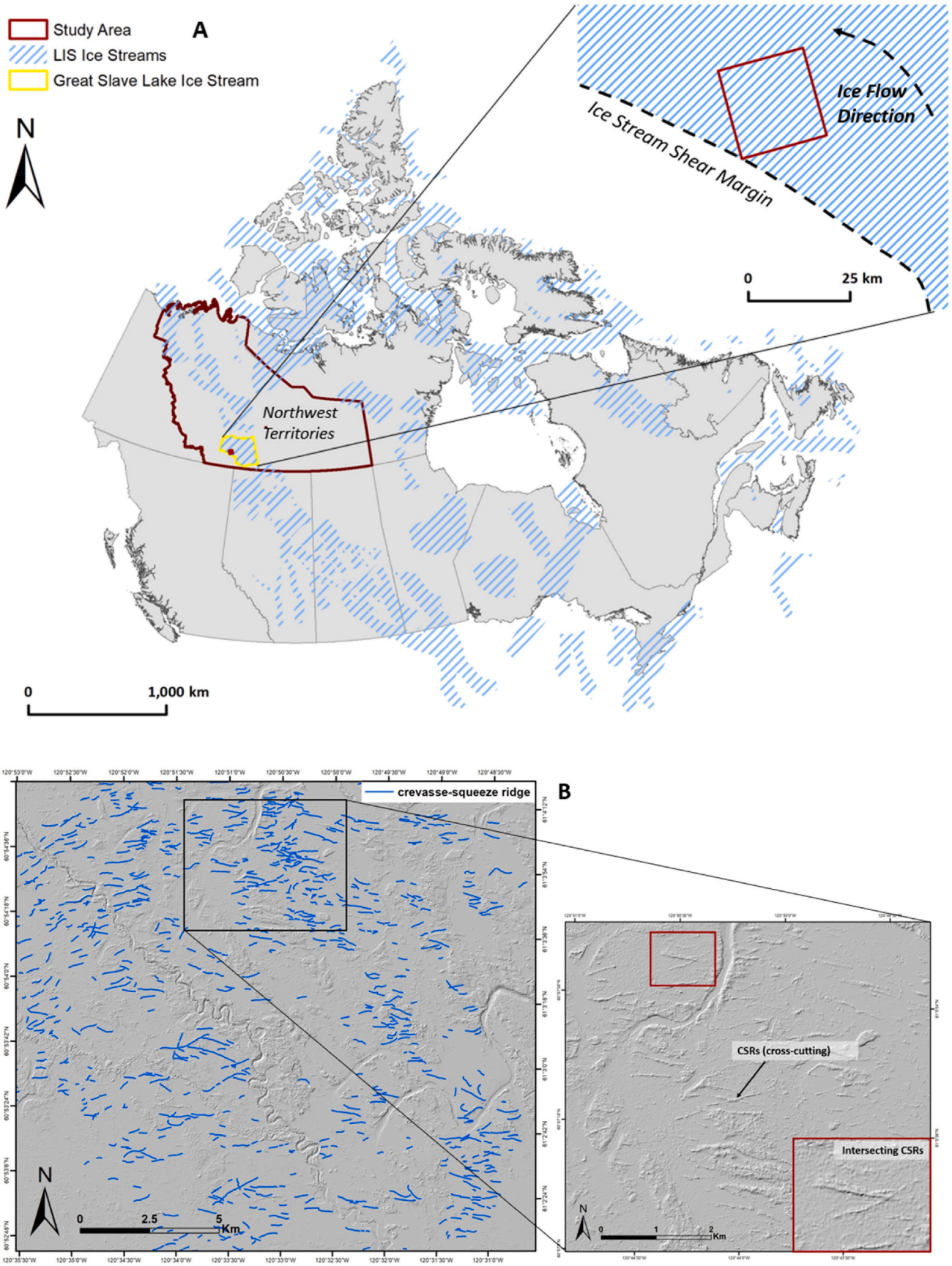

Fig. 5. A) Study area selected for CSR data collection. Location: Great Slave Lake palaeo-ice stream, Northwest Territories, Canada [ice stream data source: Margold et al., 2015]. Location map shows the study area situated inside of the shear margin of the Great Slave Lake ice stream. B) Hillshaded DEM showing mapping extent of CSRs at study area. The imagery shows CSRs arranged in a linear, sometimes cross-cutting swarm. [DEM source: ArcticDEM – Porter et al., 2018].

feature morphometric assessment. This results in a toolbox that can provide: (1) 3D morphometry at high-resolution segmented intervals, which is valuable for detailed landform analysis; and (2) a powerful method by which to compare detailed morphometrics between individual features. The ability to rapidly generate 3D morphometric data for large sample sizes is also advantageous for investigating patterns in spatial distribution, either at smaller scales, along individual feature lengths, or at macroscales across wider landscape coverages. The toolbox workflow is as follows:

1. Data preparation (digitisation of target features)
2. Execution of the primary tool '3D Morphometry Tool'
3. Undertaking of quality control checks and refining of primary output data
4. Execution of the secondary tool 'Average Feature Morphometry'
5. Undertaking further analysis of the calculated morphometry data as required

4.1. Data preparation

In this study, we define ridges identified in the DGM fields as 'prominent' when they are regularly spaced, well-defined and laterally continuous, and as 'intermediate' when they are laterally discontinuous, less defined in height and width, and have no sign of regularity to adjacent ridges (Fig. 1). DEMs with 2 m horizontal resolution, were obtained for each study area (National Land Survey of Finland, 6/2023; ArcticDEM – Porter et al., 2018). The *absolute* vertical accuracy of Finnish LiDAR data is ± 0.1 m (National Land Survey of Finland, 6/2023) and 1.6 m for the ArcticDEM (Natural Resources Canada, 2015). In this study, however, the *absolute* accuracy (i.e. correct spatial positions) are not important. Rather, it is the *relative* accuracy (the reliability of internal measurements from the DEM) that determine the reliability of our data. The differences in *relative* vertical accuracy between the two datasets were determined by conducting a test to compare calculated height across a set of mapped DGMs in SW Finland from both data sources. 573 transects were compared across an area of ~4 km^2. A Wilcoxon signed-rank test showed a small (relative to the feature height) but statistically significant mean difference of 0.79 m between the two datasets *($z = -12.8$, $p < .001$, $r=-0.05$)* (Supplementary, Fig. 1). The results showed that 76% of the calculated LiDAR heights were greater than those calculated from the ArcticDEM data.

Data collection was performed manually by carefully scanning each DEM for evidence of target features (e.g. ridges that could be qualitatively interpreted as DGMs/CSRs). The quality of the input data determines the quality of the calculated morphometrics. As such, a dual rendering of each DEM dataset was performed producing a hillshade using two different azimuths to reduce shadow bias (Smith and Clark, 2005), and a slope rendering to maximise the identification of central and lateral slope breaks for each feature (Chandler et al., 2018). Therefore, to identify the target features and maximise mapping accuracy, both hillshade and slope renderings of the DEMs were produced. The hillshade was used to identify target features and the slope map was used to accurately identify the break in central and lateral slopes. Crestlines and outlines of each identified feature were carefully mapped and stored as two ArcGIS shapefiles, a polyline shapefile for the crestlines, and a polygon shapefile for the outlines (Supplementary, Fig. 2).

4.2. Geoprocessing methods and morphometry calculation

Upon primary tool execution, each individually mapped crestline and outline is given a relative identification linking it to the target feature. Transects are then produced along each digitised crestline at user-defined intervals at an orientation of 90° to the crestline (Fig. 6A). The interval used in this study was 20 m. Elevation points are produced at three intersectional locations along each transect: at either side of the digitised outlines and the intersection at the crestline (Fig. 6B).

Basic geometric information is calculated for each feature from the outline and crestline shapefiles. A footprint area is calculated from digitised outlines, and length and sinuosity are calculated from digitised crestlines (Fig. 6A). 3D morphometric data (height, width, slope, asymmetry, cross-sectional area, and cross-sectional volume) are extracted and calculated along each transect (Fig. 6B and C). The architecture of GIS tool integration can be seen in Supplementary, Fig. 3. 3D morphometric calculations are detailed in Supplementary, Table 1.

4.3. Tool operation and required inputs

Once all identified features were digitised, the '3D Morphometry Toolbox' was imported into the general ArcGIS 'ArcToolbox' ready for execution. Each dataset (e.g. DGM landforms and CSR landforms) was executed separately.

4.3.1. The primary tool

The primary tool '3D Morphometry Tool' requires: a polygon shapefile (.shp) containing digitised outlines of the identified target features, a polyline shapefile (.shp) containing digitised crestlines of the identified target features, a DEM of the study area (.tif), and a specified 'Output Folder' to store generated outputs. The file path to the 'Output Folder' must not contain any spaces. The 'Output Folder' should be refreshed after each tool has completed execution. The primary tool generates cross-profile transects that provide detailed morphometrics along a feature's length. These transects can be tailored to the users requirements.

The primary tool requires two additional user-specified parameters in order to tailor the transects: (1) transect intervals (units: meters), which is the distance the user desires to set between each transect; and (2) transect length (units: meters), which is the length of each individual transect (NB: transect lengths should be set at a length which extends beyond the entire width of the digitised outlines as these will be clipped to the outline extent upon running the tool). Note: the run time of the tool is dependent on the size of the input dataset and the number of transects specified to be generated, as well as the specification of the computer used.

4.3.2. The secondary tool

The secondary tool 'Average Feature Morphometry' requires: the generated 'Transect_Morphometry.shp' file, the generated 'Feature_Morphometry.shp' file, the original 'Feature Outline' shapefile, and the file path to the specified 'Output Folder'.

4.4. Generated outputs

4.4.1. Primary tool '3D morphometry tool'

The executed primary tool provides outputs in geospatial and graphical formats.

Specific outputs include:

1) A shapefile ('Transect_Morphometry.shp'). This file contains all calculated 3D morphometric data for each transect segment (e.g. feature ID, crestline elevation, base terrain elevation, landform height, slope, width, asymmetry, cross-sectional area and cross-sectional volume) (Supplementary, Table 2). An example of generated transects can be seen in Fig. 7.

2) A shapefile containing merged outlines and crestlines ('Feature_Morphometry.shp'). The attribute table of this shapefile contains morphometric information (feature ID, length, area, and sinuosity). Each mapped feature is given a feature identification ('Feature_ID') and related crestlines, outlines and generated transects are associated accordingly.

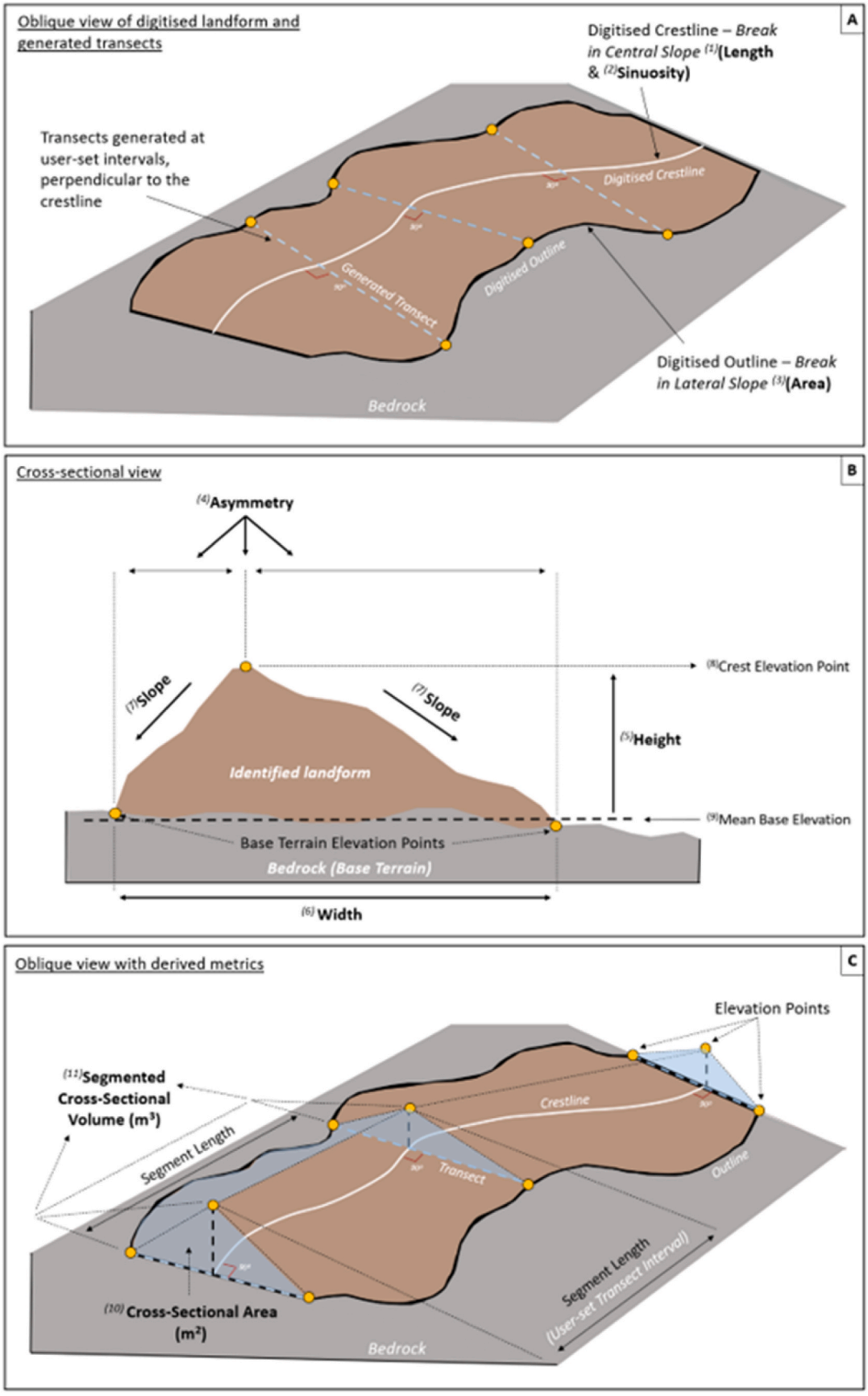

(caption on next page)

Fig. 6. A) Oblique view of digitised landform and generated transects. Basic morphometrics are calculated from outlines and crestlines (e.g. length, sinuosity and footprint area). B) Cross-sectional view of a digitised landscape feature highlighting the three elevation points along each transect. Asymmetry is calculated along each transect at the point of crestline intersection. A mean average base terrain elevation is calculated from the 'Base Terrain Elevation Points' (e.g. the two end points of each transect located on the crestline). The height is calculated from the difference between the 'Mean Base Elevation' and the 'Crestline Elevation'. Width is calculated based on the extent of the digitised outlines. C) Oblique view of a digitised landscape feature with derived metrics. Cross-sectional area is calculated based on the principles of a triangular prism (e.g. 0.5 × width (transect length) x height). Cross-sectional volume is calculated for each 'transect segment' (e.g. cross-sectional area x segment length (transect interval)). Each morphometric parameter calculated by the tool is numbered (superscript); refer to Supplementary Table 1 for details.

Table 1
Summary statistics of quantified prominent De Geer Moraine morphometrics.

	Height (m)	Width (m)	Slope (°)	Asymmetry	Length (m)	Sinuosity
Mean	1.05	24.33	10.07	0.54	213.49	1.034
Median	0.89	22.62	9.22	0.55	184	1.025
Min	0.1	1.99	0.72	0.009	28	1
Max	5.87	79.52	41.53	1	953	1.29
Std. Dev	0.72	8.92	4.75	0.10	127.45	0.03
Kurtosis	2.32	4.48	1.16	0.28	3.85	8.12
Skewness	1.30	1.60	0.98	−0.12	1.63	2.34
Variance	0.52	79.62	22.55	0.01	16242.39	0.001

Table 2
Summary statistics of quantified intermediate De Geer moraine morphometrics.

	Height (m)	Width (m)	Slope (°)	Asymmetry	Length (m)	Sinuosity
Mean	0.87	18.38	10.55	0.50	82.45	1.029
Median	0.72	17.46	9.89	0.51	69	1.0152
Min	0.1	1.08	0.57	0.002	12	1
Max	5.54	78.86	35.19	0.97	448	1.26
Std. Dev	0.64	6.37	4.63	0.11	51.99	0.04
Kurtosis	3.92	7.79	0.63	0.65	5.98	7.05
Skewness	1.56	1.66	0.78	−0.11	1.99	2.35
Variance	0.41	40.62	21.47	0.01	2703.10	0.001

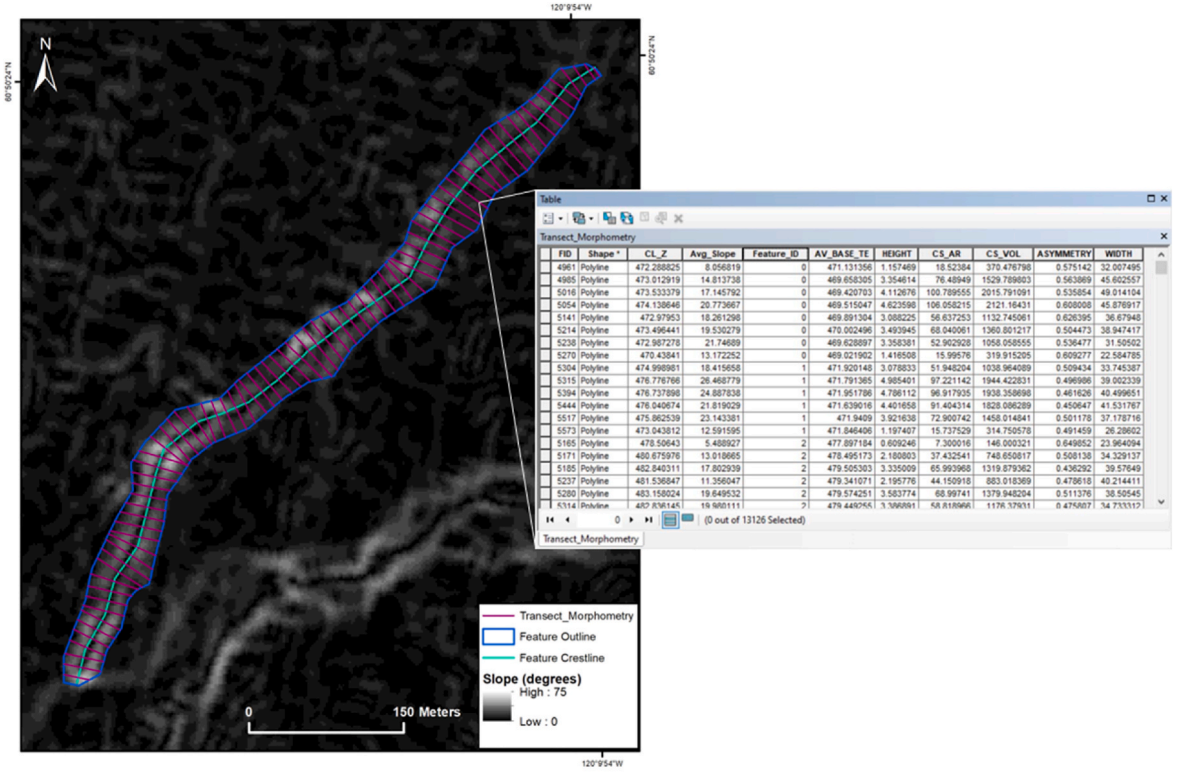

Fig. 7. Example of generated transects upon execution of the primary tool '3D-Morphometry-Tool' with inset attribute table showing calculated morphometrics per transect. Transects are oriented 90° to the feature crestline and are spaced at 10 m intervals. [Slope rendered DEM source: ArcticDEM - Porter et al., 2018].

3) A series of summary histograms for each calculated transect morphometric (i.e., 'Asymmetry.png', 'Average_Slope.png', 'Cross_-Sectional_Area.png', 'Cross_Sectional_Volume.png', 'Height.png' and 'Width.png') (Supplementary, Fig. 4).

4.4.2. Quality control checks

Upon primary tool execution, quality control checks should be undertaken. This involves reviewing the calculated transect morphometrics ('Transect_Morphometry.shp') and observing the form and location of the transects generated by the tool.

The sign (±) of the morphometric variable's height, cross-sectional area, and volume, will determine whether the feature is positive relief (positive values) or negative relief (negative values). It is advised to sort the data by one of these parameters to ensure that the values are what was expected (it can be possible to digitise incorrect features, for example).

Distorted transect placements may also appear, usually due to manual mapping errors or highly sinuous landforms (Supplementary, Fig. 5). These can generally be identified by anomalous values within the ('Transect_Morphometry.shp') attribute table. It is advised that any distorted results are removed from the data to mitigate influential anomalies and interpretative errors. It is important to note that once data is removed from the calculated transect morphometry shapefile, the preliminary summary histograms will no longer be representative of the data.

4.4.3. Secondary tool 'Average Feature Morphometry'

The executed secondary tool calculates the mean of each transect morphometric per parent feature. This information is populated in a newly generated 'Av_Feature_Morphometry.shp' shapefile containing landform attribute data: area, sinuosity, length, average crestline elevation, average base terrain elevation, average height, average asymmetry, average slope, average width, and total volume per parent landform (Supplementary, Table 3).

4.5. Script execution

The tools are written in Python [v2.7] and incorporate Python libraries from 'ArcPy' [ArcGIS 10.0–10.6], os, 'Pandas' [McKinney and others, 2010], and embeds Python code for tools, 'Transect2.0' [created by Mateus Vidotti Ferreira], and 'Create Points on Lines' [created by Ian Broad]. The toolbox needs to be downloaded from the GitHub repository (https://github.com/gwynrivers/3D_Morphometry_Toolbox) and imported into the general ArcGIS 'ArcToolbox' workspace prior to use. An instructional guide and demonstration video are also available for user reference.

4.6. Software requirements and availability

The toolbox is intended to work within ArcGIS 10.1 [ArcMap, 1995] and subsequent versions (including ArcGIS Pro [ESRI Inc, 2020]). A '3D Analyst' and 'Spatial Analyst' license is required. The toolbox can be downloaded from the GitHub repository as detailed in the appended supplementary information.

5. Results

2581 prominent DGMs and 1385 intermediate DGMs were identified across south-west Finland (Figs. 4), and 1159 CSRs were identified for the study area in NWT, Canada (Fig. 5). 27 753 transects were generated across the prominent DGM features, 6118 transects were generated across the intermediate DGM features and 18 564 transects were generated across the CSR features (post quality control checks). It should be noted that in some instances, intermediate DGMs were found to be of very low amplitude and therefore mapping accurate outlines was not feasible. This will therefore limit analysis of wider spatial distribution, however, the data acquired will be valuable for comparative morphometric assessments and single feature variability assessments.

Once the 3D morphometric data had been generated for each dataset, comparative assessments were undertaken. Transect data was used to assess height, width, slope, and asymmetry. Average feature data was used to assess length and sinuosity. Extreme values that deviated greatly from the overall dataset were removed.

5.1. Summary statistics

Summary statistics of each quantified landform morphometric are provided in Tables 1–3; and Fig. 8. We now describe each metric in turn.

Results from each landform group across all morphometrics are positively skewed, with the exception of asymmetry, which show negative skewness values across all landform groups (prominent DGM -0.12; intermediate DGMs −0.11; CSRs −0.03). Whilst asymmetry is similar across all landform groups, prominent DGMs appear slightly more asymmetrical; this can be seen by comparison of the IQR where prominent DGMs show slightly greater median and mean values, and the third quartile exceeds 0.6 (Fig. 8).

CSRs show a positive skewness for width, that is less positively skewed than height. Across all landform groups, CSRs show the most variability across all morphometrics, with the exception of asymmetry and sinuosity - this is highlighted in the results for standard error (Fig. 8G and H). Intermediate DGMs overall have the lowest values and least variability across each morphometric, particularly for length, width, and height.

Sinuosity values are similar between prominent and intermediate DGMs, however, the IQR of intermediate DGMs extends lower than prominent DGMs showing that 50 % of the intermediate DGM sample are less sinuous than prominent DGMs. CSRs are the least sinuous landform across each group.

CSRs appear to be the greatest in length across all landform groups with the most variability. However, this could be due to the discontinuous nature of prominent DGMs, which commonly consist of multiple fragments with small gaps, which would be significantly longer if taken together. The same is not true of CSRs.

Overall, the results show that the prominent DGMs are more sinuous, and slightly more asymmetrical than CSRs. CSRs are wider, higher, straighter, and more symmetrical. Intermediate DGMs are shorter, narrower, and less sinuous than prominent DGMs, but more sinuous than CSRs.

The differences in calculated height between the DGMs and CSRs are substantially greater than the mean difference between the different DEM sources as reported above (i.e. 0.79 m; Section 4.1) (Supplementary, Fig. 1), confirming that the differences are genuine and not an artifact of the underlying data.

5.2. Statistical tests

Following the contrasts and similarities highlighted in the previous section, a parametric, two-tailed, z-test was conducted for each metric to test for the statistical significance of any differences between mean averages across each landform group. Results are summarized in Table 4.

The results from the statistical analyses confirm that there is a statistically significant difference between each of the landform groups, with the exception of sinuosity, whereby intermediate DGMs and CSRs show no statistically significant difference. This is particularly important, as whilst the summary statistics showed that some metrics had only slight differences (e.g. asymmetry), these differences are significant and provide a substantive means by which to differentiate between each landform group. Furthermore, a statistically significant difference in asymmetry, with prominent DGMs being the most asymmetrical of the landform groups, provides a justified means by which to infer formational properties, and a scientific basis by which to correctly interpret and position these landforms within a wider glacial context.

Table 3
Summary statistics of quantified CSR morphometrics.

	Height (m)	Width (m)	Slope (°)	Asymmetry	Length (m)	Sinuosity
Mean	2.73	45.30	12.62	0.49	288.66	1.028
Median	2.17	41.55	11.14	0.50	245	1.016
Min	0.1	1.10	0.24	0.004	39	1
Max	13.90	99.99	60.90	0.98	794	1.33
Std. Dev	2.18	18.44	7.53	0.09	164.69	0.04
Kurtosis	2.05	0.23	1.35	0.75	0.38	13.42
Skewness	1.33	0.74	1.05	−0.03	1	3.16
Variance	4.77	340.16	56.74	0.01	27122.15	0.002

5.3. Landform summary

Based on the quantified morphometric data, a data summary table has been created (Table 5) providing a taxonomic generalisation of each landform. Each metric range has been taken from the lower and upper whiskers presented in the summary boxplots (Fig. 8).

5.4. Spatial observations

5.4.1. Single feature variability

The calculated cross-sectional area morphometrics for each transect are visualised using a colour-graded scale (high values in red, low values in blue) to assess spatial variations and/or patterns in morphometry along a single feature's length for each landform group (Fig. 9A, B & C). Values were categorised using the ArcGIS automated natural breaks (Jenk's). The results reveal some profile variability across all landform datasets, however, the variability of CSRs appears to be greatest compared to the other landform groups (Fig. 9C). This is reflected in the standard error results (Fig. 8G and H).

A closer assessment of individual feature profile variability shows that, in some cases, the ridges are greater in size centrally along the feature profile, with values decreasing laterally (Fig. 9A and C). This is likely a representation of sustained subaerial exposure and lateral erosion. However, with respect to CSRs, it could also be a preservation of the form of the crevasse in which the CSR was deposited and may also be an indicator of the removal of lateral support following any interstitial melt and down-wasting of the surrounding ice (Rea and Evans, 2011). Generally, profile variability appears irregular across both prominent DGMs and CSRs, with sometimes greater values clustered to one side of the feature, or a section located centrally along the feature profile (Fig. 9A and C). Intermediate DGMs present the least profile variability, showing generally uniform, low-relief metrics with occasional, sporadic cross-sections of greater values (Fig. 9B).

5.4.2. Macroscale variations

To investigate wider spatial characteristics, and to test whether there are any patterns in landform distribution for key morphometric variables, a Getis-Ord Gi* cluster analysis was conducted (ArcGIS, ESRI). Hot spots (represented in red) show significant clustering of high values and cold spots (represented in blue) show significant clustering of low values. This test was performed on the total volume, average width, and average height metrics for prominent DGMs (Fig. 10) and CSRs (Fig. 11). This test was not conducted on intermediate DGMs because of the difficulties in mapping across the entire study area due to very low relief features.

The results for prominent DGMs total volume reveal a clustering of larger features in the northwest of the study area and minor clusters of both smaller and larger DGMs in the southeast (Fig. 10A). A comparison between width (Fig. 10B) and height (Fig. 10C) show the variations of morphometrics across southwest Finland, with wider DGMs located in the southeast and higher DGMs located in the northwest.

The results for CSR total volume show a cluster of larger CSRs situated in the southwest of the study area, closer to the ice stream shear margin (Fig. 11A). Clusters of smaller CSRs appear to be located further into the ice stream northeast of the study area, with minor clusters of larger CSRs located north -northwest (Fig. 11A). A comparison between width (Fig. 11B) and height (Fig. 11C) shows differences in spatial distribution. Clusters of wider CSRs (Fig. 11B) appear to be situated in the north – northeast of the study area, with large clusters of narrower CSRs located both to the south and east. CSR height clusters appear to be larger and more distinctive than CSR width, with taller CSRs situated in the southwest and shorter CSRs situated to both the east and west of the study area.

6. Discussion

6.1. Glacial dynamics - importance of DGMs & CSRs

DGMs and CSRs are useful for providing insights regarding palaeoglacial processes. Specifically, they can reveal information regarding spatiotemporal ice-marginal dynamics, ice-margin direction and/or subglacial processes. The review of literature highlights distinct similarities of morphology and distribution between DGMs and CSRs and brings attention to the issue of misinterpretation between these landforms (section 2).

As CSRs are a preservation of the spatial extent of crevasses, it should be noted that crevasses evolve and deform with ice flow. Considering contemporary crevassing studies, authors report that particularly in ice stream shear zones, crevasses can undergo a cycle of formation and rotation (Price and Whillans, 2001; Whillans and van der Veen, 2001), often described as a 'chaotic crevasse network' in contrast to the linear and geometric arrangements described in previous CSR studies (Evans et al., 2016). This chaotic assemblage has generally been related to ice stream shear margin environments and evidence of this may be found with more detailed analyses of variations in spatial patterns.

Observations have been made of CSRs in both terrestrial and submarine settings of surge-type glaciers: Iceland (Sharp, 1985; Bennett et al., 2000; Evans et al., 2007, 2016; Kjaer et al., 2008; Kurjanski et al., 2019; Schomacker et al., 2014; Jonsson et al., 2014; Clapperton, 1975; Evans and Rea, 1999), Yukon Territory, Canada (Johnson, 1975; Clark et al., 1984), Alaska (Ensminger et al., 2001), Svalbard (Boulton et al., 1996; Evans and Rea, 1999; Sobota et al., 2016; Christoffersen et al., 2005; Lovell et al., 2015; Farnsworth et al., 2016; Ottesen and Dowdeswell, 2006 & 2008; Lovell et al., 2015; Streuff et al., 2015), the Barents Sea (Solheim, 1991), and eastern Poland (Orlowska, 2022). Recent studies have also reported observations in palaeo-ice stream settings: western Canada (Evans et al., 2016), Barents Sea (Kurjanski et al., 2019), and in the Gulf of Bothnia (Greenwood et al., 2017).

The variability in setting (e.g. marine vs terrestrial environments) appears to play a role in both preservation potential and spatial distribution of CSRs. CSRs observed in marine settings tend to be larger, particularly in height, which is suggested to be due to protection from subaerial exposure and postglacial reworking (Lovell et al., 2015; Farnsworth et al., 2016; Ottesen and Dowdeswell, 2006; Boulton et al., 1996; Ottesen et al., 2008; Rea and Evans, 2011). In addition, different ice dynamic settings (i.e. surge vs ice streaming) have revealed subordinate CSR patterns which may be useful in delineating ice flow dynamics (Evans et al., 2016). This supports the inference that variations

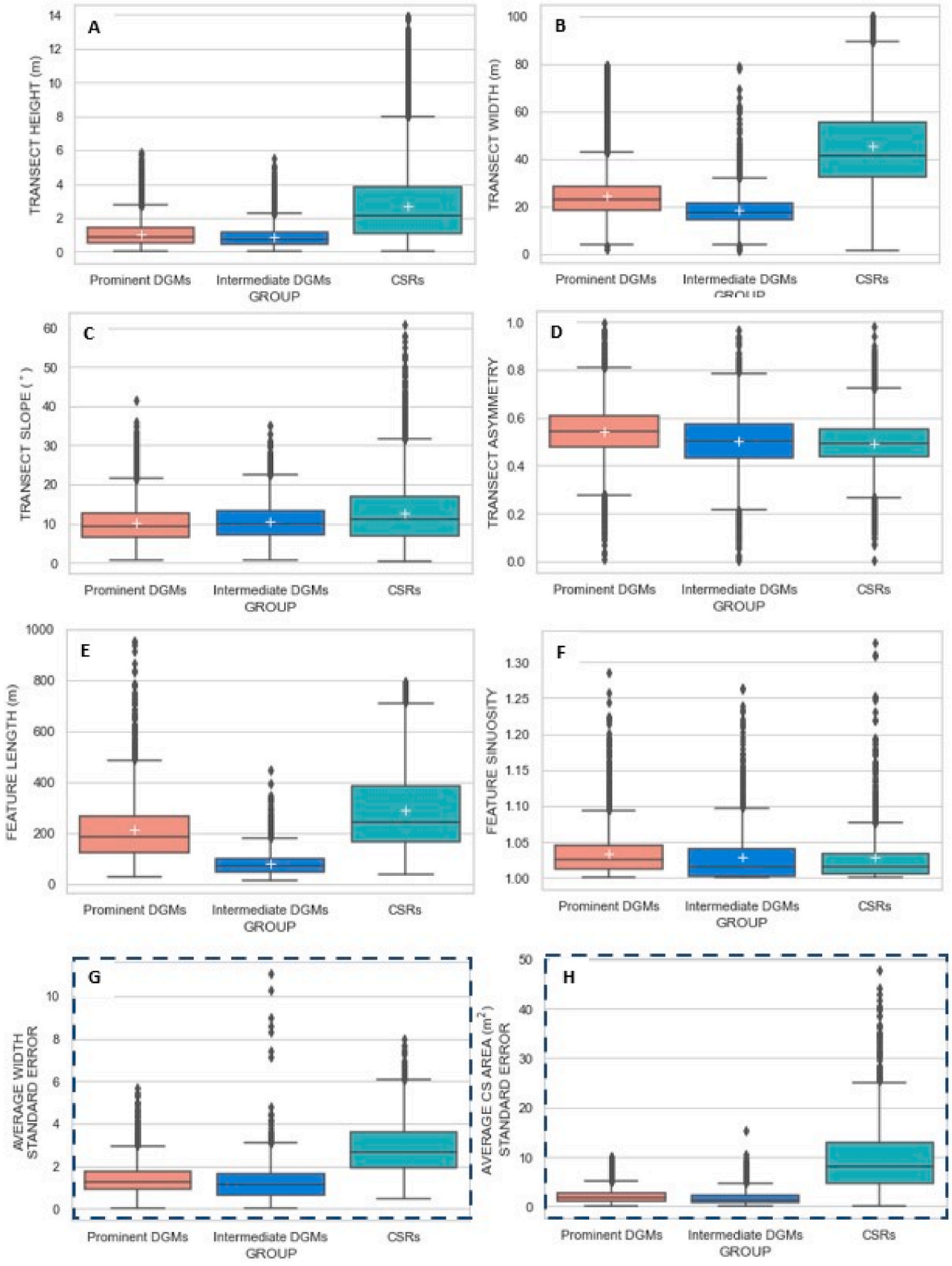

Fig. 8. A series of boxplots presenting comparative summary statistics of quantified prominent DGM, intermediate DGM and CSR morphometry data. A) Transect Height, B) Transect Width, C) Transect Average Slope, D) Transect Asymmetry, E) Feature Length, F) Feature Sinuosity, G) Average Width Standard Error, and H) Average Cross-Sectional Area Standard Error. The lower and upper whiskers represent the minimum and maximum values of the data respectively with outliers residing outside of each whisker limit, the box represents the interquartile range (IQR) (e.g. 50% of the data) with the lower limit representing the lower quartile (Q1) and the upper limit representing the upper quartile (Q3). The central interquartile line represents the median value of the dataset. The white + symbol represents the mean average value. Extreme values that extended far beyond the general dataset were removed.

Table 4
z-test results table summarising each morphometric.

Height			
	Z Statistic (Critical value: 1.96)	**Result**	**Comments**
Prominent DGMs vs CSRs	−101.04	Significant difference	CSRs greater in height
Intermediate DGMs vs CSRs	103.13	Significant difference	CSRs greater in height
Prominent DGMs vs Intermediate DGMs	19.2	Significant difference	Prominent DGMs greater in height
Width			
	Z Statistic (Critical value: 1.96)	**Result**	**Comments**
Prominent DGMs vs CSRs	−144.11	Significant difference	CSRs greater in width
Intermediate DGMs vs CSRs	170.41	Significant difference	CSRs greater in width
Prominent DGMs vs Intermediate DGMs	60.98	Significant difference	Prominent DGMs greater in width
Slope			
	Z Statistic (Critical value: 1.96)	**Result**	**Comments**
Prominent DGMs vs CSRs	−41.04	Significant difference	CSRs greater slope angles
Intermediate DGMs vs CSRs	25.5	Significant difference	CSRs greater slope angles
Prominent DGMs vs Intermediate DGMs	−7.4	Significant difference	Intermediate DGMs slightly greater slope angles
Length			
	Z Statistic (Critical value: 1.96)	**Result**	**Comments**
Prominent DGMs vs CSRs	−13.80	Significant difference	CSRs greater in length
Intermediate DGMs vs CSRs	40.99	Significant difference	CSRs greater in length
Prominent DGMs vs Intermediate DGMs	45.6	Significant difference	Prominent DGMs greater in length
Asymmetry			
	Z Statistic (Critical value: 1.96)	**Result**	**Comments**
Prominent DGMs vs CSRs	54.26	Significant difference	Prominent DGMs greater asymmetry values
Intermediate DGMs vs CSRs	−5.14	Significant difference	Intermediate DGMs greater asymmetry values
Prominent DGMs vs Intermediate DGMs	26.76	Significant difference	Prominent DGMs greater asymmetry values
Sinuosity			
	Z Statistic (Critical value: 1.96)	**Result**	**Comments**
Prominent DGMs vs CSRs	4.4	Significant difference	Prominent DGMs greater in sinuosity
Intermediate DGMs vs CSRs	−0.47	No significant difference	Similar sinuosity values
Prominent DGMs vs Intermediate DGMs	4.13	Significant difference	Prominent DGMs greater in sinuosity

Table 5
Preliminary landform summary table providing a taxonomic generalisation of prominent DGMs, intermediate DGMs and CSRs.

Landform Summary Table			
	Prominent DGMs	Intermediate DGMs	CSRs
Height (m)	0.1–2.7	0.1–2.3	0.1–8
Width (m)	3.7–43	3.7–32	1.1–89
Length (m)	28–486	12–182	39–710
Slope (°)	0.7–21.6	0.6–22.5	0.2–31.7
Asymmetry	0.3–0.8	0.2–0.8	0.3–0.7
Sinuosity	1–1.09	1–1.1–	1–1.09
Volume (m^3)	29–8067	7–2206	73–58 841

in CSR spatial distribution may reflect englacial/subglacial processes such as stress regimes and hydrological pressures that would control fracturing processes (Rea and Evans, 2011). It is possible that these processes may be reflected in our hotspot analysis whereby morphometrics vary across the study area (Fig. 11). Further mapping across the entire ice stream would be valuable to investigate how the spatial distribution of CSRs may vary across the wider area.

Similarly, DGMs have also been observed in different environmental settings, however, in comparison to CSRs, observations infer that DGMs always require a sub-aqueous environment in which to form (e.g. marine or lacustrine) (Finlayson et al., 2007; Golledge and Phillips, 2008; Sinclair et al., 2018). The DGM metrics from this study are slightly larger than those reported from a valley, lacustrine setting (Golledge and Phillips, 2008), thus reflecting the marine depositional environment of southwest Finland.

6.2. *CSR morphometry indicates crevasse in-filling*

Morphometrics of the CSRs are of a similar range to those reported from previous studies (e.g. Ben-Yehoshua (2017) reported CSR metrics of 1–7 m wide, 5–45 m long and 0.5–2 m high; Cline et al. (2015) reported CSR heights ranging from 0.5 to 2.5 m; and O'Cofaigh et al. (2010) reported heights of 1–4.5 m (based on field observations) and lengths of 400–1000 m (based on Google Earth imagery)), with some individual ridges extending up to 5000 m long. Some of the CSRs from this study extend slightly larger than those reported from Ben-Yehoshua (2017) and Cline et al. (2015), showing more similarity to those described from the Maskwa Ice Stream (Evans et al., 2016) (Fig. 8).

The greater width and height of CSRs likely reflects controls of sediment supply and availability of accommodation space (e.g. a crevasse cavity). Furthermore, the greater slope angles likely represent better preservation, as well as the nature of the material (e.g. angle of repose). Whilst postglacial erosional processes such as subaerial exposure and interstitial ice melt-out can degrade CSRs (Ben-Yehoshua, 2017; Evans and Rea, 1999; Sharp, 1985), generally preservation potential is high due to ice stagnation and rapid down-wasting (Evans et al., 2016), or flotational passive retreat (Kurjanski et al., 2019). The greater width, height and slope of CSRs indicate an environment whereby depositional processes exceed erosion (e.g. crevasse infilling) (Fig. 2B and C), in contrast to a subaqueous ice-marginal environment that may be exposed to glaciofluvial reworking. The lesser amplitude of DGMs supports the inference of a minor pushing formation, for example a minor advance during winter (Fig. 2A). The differences between the two landforms support the hypothesis that DGMs are ice-marginal features and not crevasse infills.

In addition, the results show that CSRs possess a much greater variability, both between and within features, in their width, height and slope compared to DGMs (Figures: 8G & H; 9, 10 & 11). This is likely a reflection of the variable crevasse morphology in which they were formed, permitting a wider variability in the resultant fill ridges (Evans et al., 2016; Price and Whillans, 2001; Whillans and van der Veen, 2001). For example, crevasses will be wider in the centre, pinching out

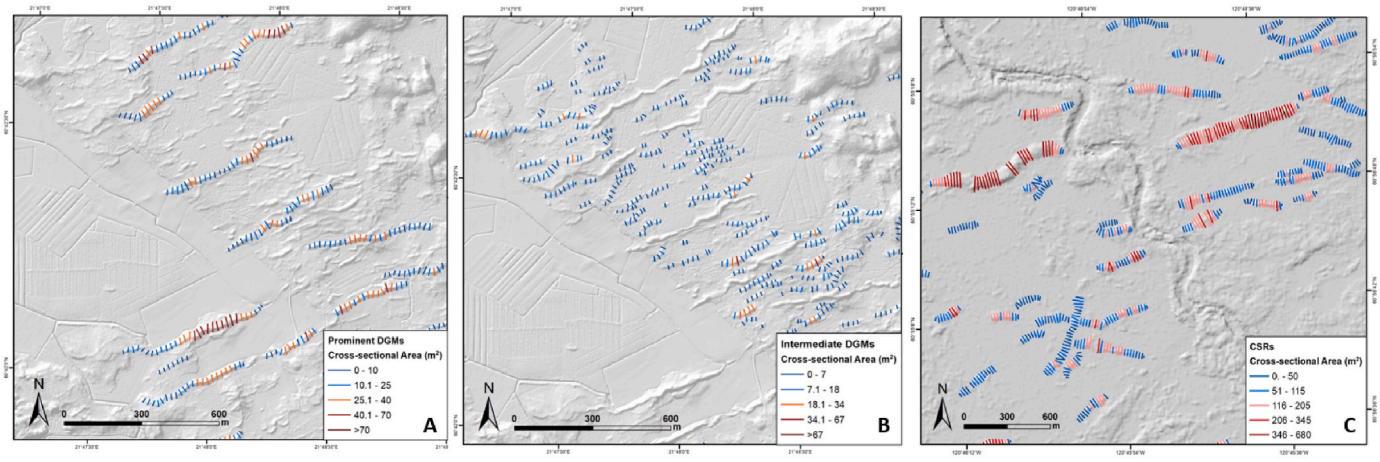

Fig. 9. Transect morphometry visualisation showing transects generated at 20 m intervals for each identified landform group: A) prominent DGMs, B) intermediate DGMs and C) CSRs. The 'cross-sectional area' calculated along each transect are shown and colour-graded to represent high (red) – low (blue) values. Each dataset were categorised using the ArcGIS automated natural breaks (Jenks) method. [DEM sources: A & B: ®National Land Survey of Finland, LiDAR digital elevation model, February 2023; C: ArcticDEM - Porter et al., 2018].

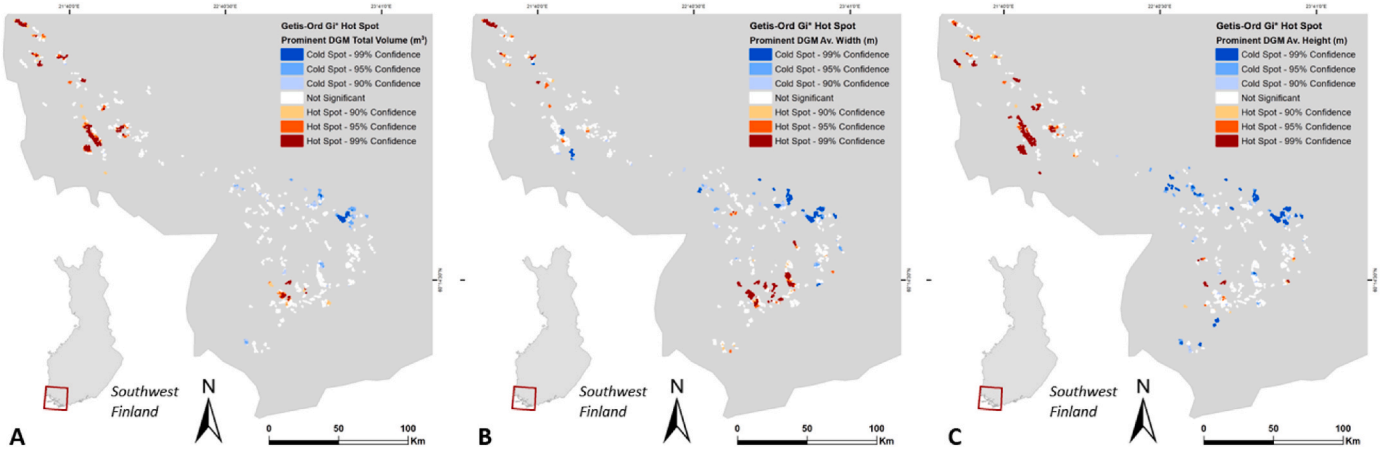

Fig. 10. Results of 'getis-ord gi* hot spot analysis'. A) Prominent DGMs total feature volume; B) prominent DGMs average feature width; and C) prominent DGMs average feature height.

at each end, thus providing variable accommodation space (Fig. 8G and H; Fig. 9C). In contrast, deposition in the ice-marginal environment would be characterised by relatively consistent width, which is controlled by the relatively uniform pushing of material.

6.3. Lateral continuity of DGMs indicates ice-marginal formation

The results show that CSRs appear to be longer than DGMs, however, this is unlikely to be a true feature of the data, as the mapped DGMs are smaller fragments of more continuous ridges. As such, lateral discontinuity is reflected in our morphometric results. If prominent DGMs segments were mapped continuously, it is likely that our results would reflect prominent DGMs that are greater in length compared to CSRs. CSRs would be restricted in length relative to their hosting crevasse, whereas DGM length would, assuming an ice-marginal pushing formation, be determined by ice marginal curvature, dynamics and reworking, which may result in lateral discontinuity and/or crenulation (Aartolahti, 1972; Ottesen et al., 2008; Linden and Moller, 2005).

The length of CSRs, in comparison to DGMs, has previously been used as an identification characteristic, whereby authors have described CSRs not to follow a continuous lateral trend similar to DGMs, instead terminating sharply and offset with respect to each other (Kurjanski et al., 2019).

6.4. DGM asymmetry indicates ice-marginal advance

Both DGMs and CSRs have been described as either symmetrical or asymmetrical (Borgstrom, 1979; Rea and Evans, 2011). However, there is a large body of research that describe DGMs with asymmetric cross-sections, characterised by a steeper distal side related to a unidirectional push process during formation, where material is pushed forwards and then falls to form a shallow proximal slope and steep distal slope (Blake, 2000; Finlayson et al., 2007; Golledge and Phillips, 2008; Linden and Moller, 2005; Ojala et al., 2015). In contrast, CSRs have been described to have symmetrical cross-sections based on 3D seismic data (Kirkham et al., 2021) and sedimentological data (Ankerstjerne et al., 2015; Sharp, 1985). This simply reflects the typically symmetrical cross-section of the accommodation space (i.e. crevasse). Our data support these ideas, with a slight, but statistically significant, difference in asymmetry between DGMs and CSRs, with DGMs presenting slightly more asymmetrical cross-sections. It should be acknowledged that each of these landforms can display both symmetrical and asymmetrical cross-sections, however, our large scale dataset support ice-marginal formation of DGM, although sedimentological data will be important to further validate this.

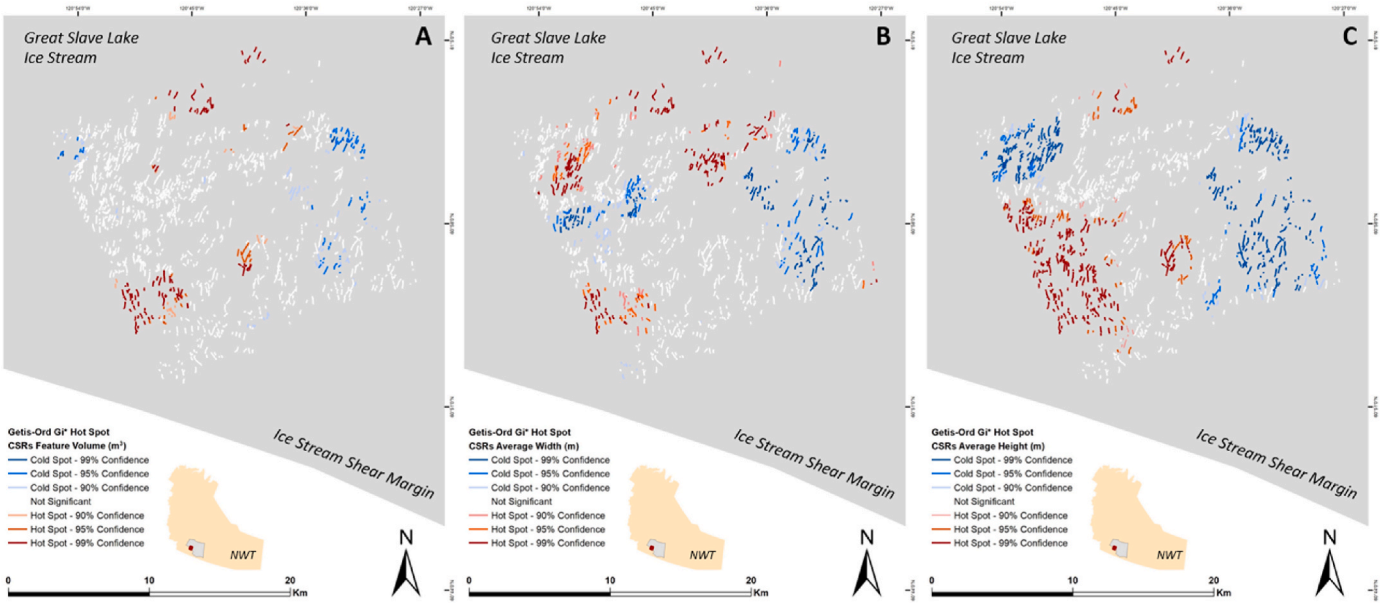

Fig. 11. Results of 'getis-ord gi* hot spot analysis'. A) Csr total feature volume; B) CSR average feature width; and C) CSR average feature height.

6.5. Wider spatial variability of prominent DGM morphometry

The variability in overall volume of prominent DGMs (Fig. 10A) across the study area may highlight several controlling factors such as: topographic controls, sediment availability, preservation potential, postglacial clay masking, water depth, elevation, rate of retreat, ice margin configuration or flow dynamics. The differences between width and height (Fig. 10B and C) could also be indicative of each of the controls described above. For example, wider, lower DGMs in the southeast may reflect a restricted sediment supply and/or differences ice configuration/flow compared to the northwest of the study area. It may also reflect greater erosional processes/slope degradation due to differences in postglacial reworkings and sub-aerial exposure.

6.6. Wider spatial variability of CSR morphometry

The spatial distribution and cluster analysis of CSRs may indicate controls related to the ice stream shear margin. The results from this study show a large cluster of larger CSRs closer to the shear margin. This is similar to CSR spatial distributions reported from previous studies (Lovell et al., 2015). As the study area is not situated directly across the shear margin, it is possible that CSR spatial distribution may reflect ice stream shear margin migration (Haseloff, 2015; Stokes, 2000). The clustered CSR spatial distribution may also highlight other controls relating to ice stream bed characteristics such as: sediment availability, topography, roughness, and lithology (Stokes, 2000). Each of these would influence stress regimes, fracturing processes, and hydrological pressures within and beneath the ice. CSRs transportation should also be acknowledged, whereby CSRs are formed within a crevasse which is then transported englacially before final deposition (Ben-Yehoshua, 2017). The CSRs in this study were not mapped for the purpose of spatial pattern analysis. Whilst some observations can be made from our data, given the various possible controls on spatial distribution, extended mapping would be required to investigate CSRs and ice stream/shear margin dynamics further.

6.7. Intermediate De Geer Moraines

Regarding geomorphological appearance, there are many different types of DGM fields in Finland and intermediate DGMs are not always present (Ojala, 2016). These ridges are observed either 1) in the spaces between regularly spaced prominent DGMs (Fig. 1E), or 2) in separate fields that have no regularly spaced prominent DGMs. The morphometric results show that these intermediate ridges are different to prominent DGMs, generally presenting as lower relief features. In addition, these intermediate DGMs show less asymmetry than that of prominent DGMs which could indicate a different formation process. It could be, for example, that they are subdued versions of prominent DGMs, or it could be that they are crevasse infills formed behind the grounding line that is marked by the prominent DGM. This warrants further investigation whereby sedimentological and geophysical data would be valuable. It should also be noted that the characteristic 'regularly spaced' properties of DGMs usually refers to prominent DGMs. Intermediate DGMs are typically positioned irregularly within the spaces between prominent DGMs. Therefore, if any temporal investigations were to be undertaken, differences between prominent and intermediate DGMs should be considered.

6.8. Applicability of the 3D morphometry toolbox

This case study has demonstrated the effective use of a newly developed 3D morphometry toolbox for the automated extraction and calculation 3D morphometric data across large scale sample sizes. This has shown how large sample sizes of a given landform may be easily quantified, with generated results that can be used as an effective classification dataset and/or means for comparative landform insights. In addition, this case study has demonstrated a flexible utility of the generated data which can be used for either detailed feature assessments, whereby individual transect segments can be analysed along a feature's length, or for wider comparative assessments to assess spatial distribution. Furthermore, the approach of a statistical 'hot spot analysis' test provides a more robust assessment of the morphometric data and allows theoretical inferences to be made, particularly with regards to landform genesis and evolution. This case study has demonstrated how this method can be used as an effective preliminary step to assess landform properties, which can then be supplemented with additional evidence such as sedimentological and/or geophysical data.

Morphometric analysis is used in many areas of landscape research and environmental management, including: fluvial geomorphology (Li et al., 2022; Sarif et al., 2021; Simon et al., 2016; Re et al., 2018), glacial geomorphology (Butcher et al., 2016, 2020; Storrar et al., 2015; Ely et al., 2017), tectonic landform research (Bethell et al., 2022; Karagoz

et al., 2022; Stretch et al., 2006; White et al., 2002) mountainous landscape research (Garcia-Ruiz et al., 2000; Kaufman and Calkin, 1988; Valla et al., 2010), geoarchaeological landscape research (Abballe and Cavalazzi, 2021; Davis, 2018), and geomorphological heritage research (Gomez-Heras et al., 2019). Furthermore, a large body of research pertains to understanding and quantifying the morphometry of irregular elongated landforms such as eskers (e.g. Storrar et al., 2015; Butcher et al., 2016; Butcher et al., 2019; Frydrych, 2022), river channels (Li et al., 2022; Sarif et al., 2021; Soar et al., 2017; Xie et al., 2018), moraines (Finlayson and Bradwell, 2008; Dunlop, 2004; Kaufman and Calkin, 1988), crevasse squeeze ridges (Ben-Yehoshua, 2017; Evans et al., 2016), inverted fluvial channels (Valla et al., 2010), palaeochannels (Re et al., 2018), tectonic landforms such as volcanic structures (Scheidegger, 2002; Stretch et al., 2006; Székely and Karátson, 2004; White et al., 2002) and wrinkle ridges (Bethell et al., 2022; Karagoz et al., 2022; Kreslavsky and Basilevsky, 1998; Plescia, 1993). This highlights a wide demand for automated morphometry methods towards which this 3D morphometry toolbox may be advantageous.

The 3D morphometry toolbox may be utilized for the measurement of any elongated landscape feature for which users require a detailed 3D morphometric assessment. As such, application is not limited by discipline area and may extend to a wide range of studies, including surveying of artificial landscape features in the built environment, such as railway embankments. Furthermore, this toolbox may be used to capture a single 3D morphometric assessment of a landscape feature, which may be useful for landform classification and/or to enhance feature diagnostic criteria. Alternatively, the toolbox may be applied as a repeated monitoring method with which to analyse evolutionary properties. This may be particularly useful in contemporary, fluvial settings, for example. The toolbox can easily be applied to negative-relief landscape features (e.g. river channels) by simply switching the sign of height, cross-sectional area and volume values.

7. Conclusions

This paper presents a case study demonstrating a new method of automated 3D morphometric calculation for elongate ridge morphology. This method was used as an effective means by which to efficiently extract and calculate large sample sizes of 3D morphometric data whereby a comparative assessment of landform morphologies could then be undertaken.

Specifically, this method was used to acquire large scale, high-resolution 3D morphometric datasets of both DGM and CSR landforms. The data provides accurate morphometric quantification and a robust dataset with which to undertake comparative landform assessments. The results indicated key differences between DGM and CSR whereby CSRs are taller and wider than DGMs, reflecting enhanced sediment availability and accommodation space in crevasses, compared with ice-marginal pushing of pre-existing sediment for DGM formation. The results also revealed a statistically significant difference in profile asymmetry, whereby DGMs possess a more asymmetric cross-section compared to CSRs, supporting DGM formation by unidirectional pushing in an ice marginal/grounding line environment rather than infilling of crevasses. This is further supported by the greater sinuosity of DGMs compared to CSRs. This is explained by CSRs being limited to the dimensions and planform geometry of their host crevasses, which will tend to be relatively straight, compared with ice margins, which are subject to more crenulation and therefore produce more sinuous landforms. For similar reasons, CSRs also exhibit more variable height and width, since their host crevasses are typically wider in the centre and pinch out at the ends, unlike an ice margin which will tend to produce DGMs of rather consistent width/height. As such, this high-resolution, large scale morphometric data provides a powerful foundation by which to investigate genesis properties further. This information could then be supplemented with sedimentological and/or geophysical data to ascertain a more robust classification of each landform.

The toolbox may be used for the measurement of any elongated landscape feature where users require a detailed 3D morphometric assessment. Application may extend to a wide range of studies, including: fluvial geomorphology, glacial geomorphology, tectonic landform research, mountainous landscape research, geoarchaeological landscape research, geomorphological heritage research, as well as surveying of artificial landscape features in the built environment, such as railway embankments.

In addition, the toolbox may be used to capture a single 3D morphometric assessment of a landscape feature or applied as a repeated monitoring method in which to analyse dynamic changes. The toolbox may also be applied to negative-relief landscape features (e.g. river channels). It is intended that this tool be accessible for research and industry GIS users ranging from novice to advanced user levels. The 3D Morphometry Toolbox Python script is open-access and can be downloaded from the GitHub repository as detailed in the appended supplementary information. The script may be further developed to meet user-specific requirements, if desired.

Authorship contribution statement

Gwyneth E. Rivers[a]: contributed to the development of the methods, the development of the programming, the testing of the morphometry tool, the data collection and analysis, and the writing and editing of the manuscript. Robert D. Storrar[b]: contributed to the development of the methods, data collection and analysis, the testing of the morphometry tool and the writing and editing of the manuscript. Andrew H. Jones[c]: contributed to the development of the methods, the development of the programming, the testing of the morphometry tool and the writing and editing of the manuscript. Antti E. K. Ojala[d] contributed to data collection and analysis, and the writing and editing of the manuscript.

Declaration of competing interest

The authors declare that they have no known competing financial interests or personal relationships that could have appeared to influence the work reported in this paper.

Data availability

A link to the data/code is shared in the code availability section of the manuscript.

Acknowledgments

This research is funded by a Ph.D. GTA studentship awarded by Sheffield Hallam University.

We kindly thank Colm O'Cofaigh for his editorial work, an anonymous reviewer and Sarah Greenwood for their constructive reviews of the manuscript.

Appendix A. Supplementary data

Supplementary data to this article can be found online at https://doi.org/10.1016/j.quascirev.2023.108383.

References

®National Land Survey of Finland. LiDAR Digital Elevation Model 2, 2023.
Aartolahti, T., 1972. On deglaciation in southern and western Finland. In: Societas Geographica Fenniae, vol. 114. UIN, Helsinki, BLL01010260022.
Abballe, M., Cavalazzi, M., 2021. Morphometric analysis for geoarchaeological research: from testing different methods to results verification in the romagna plain.

Archeologia a Calcolatori 32 (1), 114–136. https://doi.org/10.19282/ac.32.1.2021.07.
Andreassen, K., Winsborrow, M.C.M., Bjarnadóttir, L.R., Rüther, 2014. Ice stream retreat dynamics inferred from an assemblage of landforms in the northern Barents Sea. Quat. Sci. Rev. 92, 246–257. https://doi.org/10.1016/j.quascirev.2013.09.015.
Ankerstjerne, S., Iverson, N.R., Lagroix, F., 2015. Origin of a washboard moraine of the Des Moines Lobe inferred from sediment properties. Geomorphology 248, 452–463. https://doi.org/10.1016/j.geomorph.2015.07.019.
ArcMap, 1995. Esri Inc. ArcGIS Desktop Version 10.6.1.9270, 2018. ArcMap software by Esri. ArcGIS and ArcMapTM. www.esri.com.
Batchelor, C.L., Dowdeswell, J.A., Hogan, K.A., Larter, R.D., Parsons, E., West, O., 2019. Processes and patterns of glaciers-influenced sedimentation and recent tidewater glacier dynamics in Darbel Bay, western Antarctic Peninsula. Antactic Science 31 (4), 218–227. https://doi.org/10.1017/S0954102019000191.
Beaudry, L.M., Prichonnet, G., 1991. Late glacial De geer moraines with glaciofluvial sediment in the chapais area, quebec (Canada). Boreas 20, 377–394. ISSN: 0300-9483.
Beaudry, L.M., Prichonnet, G., 1995. Formation of De geer moraines deposited subglacially, central quebec. Géogr. Phys. Quaternaire 49 (3), 337–361. https://doi.org/10.7202/033059ar.
Ben-Yehoshua, D., 2017. Crevasse-Squeeze Ridges in Trygghamna, Svalbard. University of Iceland, Faculty of Earth Science. Retrieved from. https://hdl.handle.net/1946/26725.
Benediktsson, Í.Ö., Ingólfsson, Ó., Schomacker, A., Kjaer, K.H., 2009. Formation of submarginal and proglacial end moraines: implications of ice-flow mechanism during the 1963-64 surge of Brúarjökull, Iceland. Boreas 38, 440–457. https://doi.org/10.1111/j.1502-3885.2008.00077.x.
Benn, D.I., Evans, D.J.A., 2010. Glaciers & Glaciation, second ed. Routledge, Abingdon, Oxon, p. 734. 13: 978-0-340-90579-1.
Bennett, M.R., 2003. Ice streams as the arteries of an ice sheet: their mechanics, stability and significance. Earth Sci. Rev. 61, 309–339. https://doi.org/10.1016/S0012-8252(02)00130-7.
Bennett, M.R., Huddart, D., Waller, R.I., 2000. Glaciofluvial crevasse and conduit fills as indicators of supraglacial dewatering during a surge, Skeidararjokull, Iceland. J. Glaciol. 46 (152) https://doi.org/10.3189/172756500781833232.
Bethell, E.M., Ernst, R.E., Samson, C., 2022. Analysis of venusian wrinkle ridge morphometry using stereo-derived topography: a case study from southern eistla regio. JGR Planets 127 (5). https://doi.org/10.1029/2021JE006879.
Blake, K.P., 2000. Common origin for De Geer moraines of variable composition in Raudvassdalen, northern Norway. J. Quat. Sci. 15 (6), 633–644. ISSN: 0267-8179.
Borgstrom, I., 1979. De geer moraines in a Swedish mountain area? Geogr. Ann. Phys. Geogr. 61 (1/2), 35–42. Retrieved from: https://www.jstor.org/stable/520512.
Boulton, G.S., van der Meer, J.J.M., Hart, J., Beets, D., Ruegg, G.H.J., van der Wateren, F. M., Jarvis, J., 1996. Till and moraine emplacement in A deforming bed surge - an example from A marine environment. Quat. Sci. Rev. 15, 961–987. https://doi.org/10.1016/0277-3791(95)00091-7.
Bouvier, V., Johnson, M.D., Passe, 2015. Distribution, genesis and annual-origin of De Geer moraines in Sweden: insights revealed by LiDAR. GFF 137 (4), 319–333. https://doi.org/10.1080/11035897.2015.1089933.
Broad, I. [Create Points on Lines Tool]. Web: www.ianbroad.com.
Butcher, F.E.G., Conway, S.J., Arnold, N.S., 2016. Are the dorsa argentea on mars eskers? Icarus 275, 65–84. https://doi.org/10.1016/j.icarus.2016.03.028.
Butcher, F.E., Balme, M.R., Gallagher, C., Storrar, R.D., Conway, S.J., Arnold, N.S., Lewis, S.R., Hagermann, A., 2019. 3D morphometries of eskers on mars, and comparisons to eskers in Finland. In: 50th Lunar and Planetary Science Conference. The Woodlands, Houston, Texas, USA, pp. 18–22. Mar 2019. http://oro.open.ac.uk/59280/1/Butcher_EskerMorphometries_1874.pdf.
Butcher, F., Balme, M., Conway, S., Gallagher, C., Arnold, N., Storrar, R., Lewis, S., Hagermann, A., 2020. Morphometry of a glacier-linked esker in NW Tempe Terra, Mars, and implications for sediment-discharge dynamics of subglacial drainage. Earth Planet Sci. Lett. 542 (116325) https://doi.org/10.1016/j.epsl.2020.116325.
Chandler, B.M., Lovell, H., Boston, C.M., Lukas, S., Barr, I., Benediktsson, I., Benn, D., Clark, C., Darvill, C.M., Evans, D., Ewertowski, M., Loibl, D., Margold, M., Otto, J., Roberts, D.H., Stokes, C., Storrar, R., Stroeven, A., 2018. Glacial geomorphological mapping: a review of approaches and frameworks for best practice. Earth Sci. Rev. 185, 806–846. https://doi.org/10.1016/j.earscirev.2018.07.015.
Christoffersen, P., Piotrowski, J.A., Larsen, N.K., 2005. Basal processes beneath an Arctic glacier and their geomorphic imprint after a surge, Elisebreen, Svalbard. Quat. Res. 64, 125–137. https://doi.org/10.1016/j.yqres.2005.05.009.
Clapperton, C.M., 1975. The debris content of surging glaciers in svalbard and Iceland. J. Glaciol. 14 (72) https://doi.org/10.3189/S0022143000021924.
Clark, G.K.C., Collins, S.G., Thompson, D.E., 1984. Flow, thermal structure, and subglacial conditions of a surge-type glacier, 232-140 Can. J. Earth Sci. 21. https://doi.org/10.1139/e84-024. https://www.researchgate.net/publication/237172635_Flow_thermal_structure_and_subglacial_conditions_of_a_surge-type_glacier.
Cline, M.D., Iverson, N.R., Harding, C., 2015. Origin of washboard moraines of the des moines lobe: spatial analyses with LiDAR data. Geomorphology 246, 570–578. https://doi.org/10.1016/j.geomorph.2015.07.021.
Davis, D.S., 2018. Object-based image analysis: a review of developments and future directions of automated feature detection in landscape archaeology. Archaeol. Prospect. 26 (2), 155–163. https://doi.org/10.1002/arp.1730.
De Geer, G., 1889. Andmoraner I trakten mellan spanga och sundbyberg [end moraines in the area between spanga and sundbyberg]. GFF (Geol. Foren. Stockh. Forh.) 11 (4), 205–208. https://doi.org/10.1080/11035898909444255.
De Geer, G., 1940. Geochronologia suecia principles. Kungl. Sv. Vetenskapsakad. Handl. Tredje serien., Bd 18 (6).
Dix, J.K., Duck, R.W., 2000. A high-resolution seismic stratigraphy from a Scottish sea loch and its implications for Loch Lomond Stadial deglaciation. J. Quat. Sci. 15 (6), 645–656. ISSN: 0267-8179.
Dunlop, P., 2004. The Characteristics of Ribbed Moraine and Assessment of Theories of Their Genesis. PhD Thesis, University of Sheffield. Retrieved from. https://etheses.whiterose.ac.uk/12841/.
Ely, J.C., Clark, C.D., Spagnolo, M., Hughes, A.L.C., Stokes, C.R., 2017. Using the size and position of drumlins to understand how they grow, interact and evolve. Earth Surf. Process. Landforms 43 (2). https://doi.org/10.1002/esp.4241.
Embleton, C., King, C.A.M., 1968. Glacial and Periglacial Geomorphology. Edward Arnold (Publishers) Ltd. SBN: 7131 5377 6.
Ensminger, S.L., Alley, R.B., Evenson, E.B., Lawson, D.E., Larson, G.J., 2001. Basal-crevasse-fill origin of laminated debris bands at Matanuska Glacier, Alaska, U.S.A. J. Glaciol. 47 (158) https://doi.org/10.3189/172756501781832007.
ESRI Inc, 2020. ArcGIS Pro. ESRI Inc, Version 2.5. https://www.esri.com/en-us/arcgis/products/arcgis-pro/overview.
Evans, I.S., 2012. Geomorphometry and landform mapping: What is a landform? Geomorphology 137 (1), 94–106. https://doi.org/10.1016/j.geomorph.2010.09.029.
Evans, D.J.A., Rea, B.R., 1999. Geomorphology and sedimentology of surging glaciers: a land-systems approach. In: Annals of Glaciology, vol. 28. International Glaciological Society. https://doi.org/10.3189/172756499781821823.
Evans, D.J.A., Twigg, D.R., Rea, B.R., Shand, M., 2007. Surficial geology and geomorphology of the Bruarjokull surging glacier landsystem. J. Maps 3 (1), 349–367. https://doi.org/10.1080/jom.2007.9710850.
Evans, D.J.A., Storrar, R.D., Rea, B.R., 2016. Crevasse-squeeze ridge corridors: Diagnostic features of late-stage palaeo-ice stream activity. Geomorphology 258, 40–50. https://doi.org/10.1016/j.geomorph.2016.01.017.
Evans, D.J.A., Ewertowski, M., Roberts, D.H., Tomczyk, A.M., 2022. The historical emergence of a geometric and sinuous ridge network at the Horbyebreen polythermal glacier snout, Svalbard and its use in the interpretation of ancient glacial landforms. Geomorphology 406, 108213. https://doi.org/10.1016/j.geomorph.2022.108213.
Farnsworth, W.R., Ingolfsson, O., Retelle, M., Schomacker, A., 2016. Over 400 previously undocumented Svalbard surge-type glaciers identified. Geomorphology 264, 52–60. https://doi.org/10.1016/j/geomorph.2016.03.025.
Mateus Vidotti Ferreira. [Transect2.0 Tool]. (Email: mateusvidotti@yahoo.com.br).
Finlayson, A., Bradwell, T., 2008. Morphological characteristics, formation and glaciological significance of Rogen moraine in northern Scotland. Geomorphology 101 (4), 607–617. https://doi.org/10.1016/j.geomorph.2008.02.013.
Finlayson, D., Bradwell, T., Golledge, N., Merritt, J., 2007. Morphology and Significance of Transverse Ridges (De Geer Moraines) Adjacent to the Moray Firth, NE Scotland. Scot. Geogr. J. 123 (4), 257–270. https://doi.org/10.1080/14702540801968477.
Frödin, G., 1916. Über einige spätglaziale Kalbungbuchten und fluvioglaziale Estuarien im mittleren Schweden. Bull. Geol. Inst. Upsala 15, 149–174.
Frydrych, M., 2022. Morphology of eskers in Poland, southward of the Last Glacial Maximum. Geomorphology 415, 108418. https://doi.org/10.1016/j.geomorph.2022.108418.
Garcia-Ruiz, J.M., Gomez-Villar, A., Ortigosa, L., Marti-Bono, C., 2000. Morphometry of glacial cirques in the central Spanish Pyrenees. Geogr. Ann. Phys. Geogr. 82 (4), 433–442, 2000.
Golledge, N.R., Phillips, E., 2008. Sedimentology and architecture of De Geer moraines in the western Scottish Highlands, and implications for grounding-line glacier dynamics. Sediment. Geol. 208 (1–2), 1–14. https://doi.org/10.1016/j.sedgeo.2008.03.009.
Gomez-Heras, M., Ortega-Becerril, J.A., Garrote, J., Fort, R., Lopez-Gonzalez, L., 2019. Morphometric measurements of bedrock rivers at different spatial scales and applications to geomorphological heritage research. Prog. Earth Planet. Sci. 6, 29 https://doi.org/10.1186/s40645-019-0275-0.
Greenwood, S.L., Clason, C.C., Nyberg, J., Jakobsson, M., Holmlund, P., 2017. The Bothnian Sea ice stream: early Holocene retreat dynamics of the south-central Fennoscandian Ice Sheet. Boreas 46, 346–362. https://doi.org/10.1111/bor.12217. ISSN 0300-9483.
Haseloff, M., 2015. Modelling the Migration of Ice Stream Margins. The Faculty of Graduate and Postdoctoral Studies, The University of British Columbia, Vancouver. Retrieved from. https://central.bac-lac.gc.ca/.item?id=TC-BVAU-54268&op=pdf&app=Library&oclc_number=1032934150.
Hoppe, G., 1957. Problems of Glacial Morphology and the Ice Age. Geogr. Ann. 39 (1), 1–18. https://doi.org/10.1080/20014422.1957.11880892.
Hoppe, G., 1959. Glacial morphology and inland ice recession in northern Sweden. Geogr. Ann. 41, 193–212.
Hughes, A.L.C., Gyllencreutzm, R., Lohne, Ø.S., Mangerud, J., Svendsen, J.I., 2016. The last Eurasian ice sheets - a chronological database and time-slice reconstruction, DATED-1. Boreas 45, 1–45. https://doi.org/10.1111/bor.12142. ISSN 0300-9483.
Ingólfsson, Ó., Benediktsson, Ö., Schomacker, A., Kjaer, K.H., Brynjólfsson, S., Jónsson, S.A., Korsgaard, N.J., Johnson, M.D., 2016. Glacial geological studies of surge-type glaciers in Iceland – Research status and future challenges. Earth Sci. Rev. 152, 37–69. https://doi.org/10.1016/j.earscirev.2015.11.008.
Johnson, P.G., 1975. Recent Crevasse Filling At The Terminus Of The Donjek Glacier, St. Elias Mountains, Yukon Territory. Quaetiones Geographicae 2, 53 - 29. UAM.
Jonsson, S.A., Schomacker, A., Benediktsson, I.O., Ingolfsson, O., Johnson, M.D., 2014. The drumlin field and the geomorphology of the Mulajokull surge-type glacier, central Iceland. Geomorphology 207, 213–220. https://doi.org/10.1016/j,geomorph.2013.11.007.

Karagoz, O., Kenkmann, T., Wulf, G., 2022. Circum-Tharsis wrinkle ridges at Lunae Planum: Morphometry, formation, and crustal implications. Icarus 374, 114808. https://doi.org/10.1016/j.icarus.2021.114808.
Kaufman, D.S., Calkin, P.E., 1988. Morphometric Analysis of Pleistocene Glacial Deposits in the Kigluaik Mountains, Northwestern Alaska, U.S.A. Arct. Alp. Res. 20 (3), 273–284. https://doi.org/10.1080/00040851.1988.12002675.
King, C.A.M., 1982. Morphometry in Glacial Geomorphology. In: Coates, D.R. (Ed.), Glacial Geomorphology. Springer, Dordrecht. https://doi.org/10.1007/978-94-011-6491-7_5.
Kirkham, J.D., Hogan, K.A., Larter, R.D., Self, E., Games, K., Huuse, M., Stewart, M.A., Ottesen, D., Arnold, N.S., Dowdeswell, J.A., 2021. Tunney Valley Infill and Genesis Revealed by High-Resolution 3-D Seismic Data, vol. 49. The Geological Society of America, pp. 1516–1520. https://doi.org/10.1130/G49048.1.
Kjaer, K.H., Korsgaard, N.J., Schomacker, A., 2008. Impact of multiple glacier surges – a geomorphological map from Bruarjokull, East Iceland. J. Maps 4 (1), 5–20. https://doi.org/10.4113/jom.2008.91.
Kreslavsky, M.A., Basilevsky, A.T., 1998. Morphometry of wrinkle ridges on Venus: Comparison with other planets. J. Geophys. Research, Planets 103 (E5), 11103–11111. https://doi.org/10.1029/98JE00360.
Kurjanski, B., Rea, B.R., Spagnolo, M., Winsborrow, M., Cornwell, D.G., Andreassen, K., Howell, J., 2019. Morphological evidence for marine ice stream shutdown, central Barents Sea. Mar. Geol. 414, 64–76. https://doi.org/10.1016/j.margeo.2019.05.001.
Larsen, E., Longva, O., Follestad, B.A., 1991. Formation of De Geer moraines and implications for deglaciation dynamics. J. Quat. Sci. 6 (4), 263–277. ISSN: 0267-8179.
Li, Y., 2020. GIS and Remote Sensing Applications in Geomorphology. Geography. https://doi.org/10.1093/OBO/9780199784002-0219. http://WWW.OXFORDBIBLIOGRAPHIES.COM/VIEW/DOCUMENT/OBO-9780199874002/OBO-9780199874002-0219.XML. Retrieved from.
Li, Z., Yan, C., Boota, M.W., 2022. Review and outlook of river morphology expression. J. Water and Clim. Change 13 (4), 1725–1747. https://doi.org/10.2166/wcc.2022.449.
Linden, M., Moller, P., 2005. Marginal formation of De Geer moraines and their implications to the dynamics of grounding-line recession. J. Quat. Sci. 20 (2), 113–133. https://doi.org/10.1002/jqs.902. ISSN: 0267-8179.
Lovell, H., Fleming, E.J., Benn, D.I., Hubbard, B., Lukas, S., Rea, B.R., Noormets, R., Flink, A.E., 2015. Debris entrainment and landform genesis during tidewater glacier surges. Journal of Geophysical Research. Earth Surf. 120, 1574–1595. https://doi.org/10.1002/2015JF003509.
Lundqvist, J., 1981. Moraine Morphology - terminological remarks and regional aspects. Geogr. Ann. Phys. Geogr. 63 (3–4), 127–138. Retrieved from. https://www.jstor.org/stable/520824.
Mäkinen, K., Palmu, J.-P., Teeriaho, J., Rönty, H., Rauhaniemi, T., Jarva, J., 2007. Nationally valuable moraine formations. The Finnish Environment 14/2007 Ministry of the Environment.
Mangerud, J., Hughes, A.L.C., Johnson, M.D., Lunkka, J.P., 2022. The Fennoscandian Ice Sheet during the Younger Dryas Stadial. European Glacial Landscapes. The Last Deglaciation 46, 437–452. https://doi.org/10.1016/B978-0-323-91899-2.00060-7.
Margold, M., Stokes, C.R., Clark, C.D., Kleman, J., 2015. Ice streams in the Laurentide Ice Sheet: a new mapping inventory. J. Maps 11 (3), 380–395, 10.1080/17445647.2014.912036.
Mawdsley, J.B., 1963. The wash-board moraines of the Opawica-Chibougamau area, Quebec. Roy. Soc. Can. Trans., Ser. 3, 9–12, 30(4).
McKinney, W., others, 2010. Pandas - Data Structures for Statistical Computing in Python. In: van der Walt, Stefan, Millman, Jarrod (Eds.), Proceedings of the 9th Python in Science Conference, vol. 445, pp. 56–61. https://doi.org/10.25080/Majora-92bf1922-00a.
Möller, H., 1962. Annuella och interannuella ändmoräner (Annual and interannual end moraines). GFF 84, 134–143. https://doi.org/10.1080/11035896209449211.
Natural Resources Canada, 2015. High Resolution Digital Elevation Model (HRDEM). Product Specifications. Edition 1.4. Government of Canda. Retrieved from: https://ftp.maps.canada.ca/pub/elevation/dem_mne/highresolution_hauteresolution/HRDEM_Product_Specification.pdf.
Norris, S.L., Evans, D.J.A., Ó, Cofaigh, C., 2018. Geomorphology and till architecture of terrestrial palaeo-ice streams of the southwest Laurentide Ice Sheet: A borehole stratigraphic approach. Quaternary Science Reviews 186, 186–214. https://doi.org/10.1016/j.quascirev.2017.12.018.
Ó Cofaigh, C., Evans, D.J.A., Smith, I.R., 2010. Large-scale reorganistaion and sedimentation of terrestrial ice-streams during a single glacial cycle. Geol. Soc. Am. Bull 122, 743–756. https://doi.org/10.1130/b26476.1.
Ojala, A.E.K., 2016. Appearance of De Geer moraines in southern and western Finland – Implications for reconstructing glacier retreat dynamics. Geomorphology 255, 16–25. https://doi.org/10.1016/j.geomorph.2015.12.005.
Ojala, A.E.K., Putkinen, N., Palmu, J.P., Nenonen, K., 2015. Characterization of De Geer moraines in Finland based on LiDAR DEM mapping. GFF 137 (4), 304–318. https://doi.org/10.1080/11035897.2015.1050449.
Orlowska, A., 2022. Crevasse-fill forms – Bridging the gap in glacial geomorphology between East and West based on a case study from eastern Poland. Quat. Int. 617, 59–72. https://doi.org/10.1016/j.quaint.2021.08.004.
Ottesen, D., Dowdeswell, J.A., 2006. Assemblages of submarine landforms produced by tidewater glaciers in Svalbard. J. Geophys. Res. 111 (F01016) https://doi.org/10.1029/2005JF000330.
Ottesen, D., Dowdeswell, J.A., Benn, D.I., Kristensen, L., Christiansen, H.H., Christensen, O., Hansen, L., Lebesbye, E., Forwick, M., Vorren, T.O., 2008. Submarine landforms characteristic of glacier surges in two Spitsbergen fjords. Quat. Sci. Rev. 27, 1583–1599. https://doi.org/10.1016/j.quascirev.2008.05.007.
Palmu, J.-P., Ojala, A.E.K., Virtasalo, J., Putkinen, N., Kohonen, J., 2021. Classification System of Superficial (Quaternary) Geologic Units in Finland, vol. 412. Geological Survey of Finland, Bulletin, pp. 115–144. Retrieved from. https://tupa.gtk.fi/julkaisu/bulletin/bt_412.pdf.
Pike, R.J., Evans, I.S., Hengl, T., 2009. Chapter 1 Geomorphometry: A Brief Guide. Dev. Soil Sci. 33, 3–30. https://doi.org/10.1016/S0166-2481(08)00001-9.
Plescia, J.B., 1993. Wrinkle ridges of Arcadia Planitia, Mars. J. Geophys. Res. 98 (E8), 15049–15059. https://doi.org/10.1029/93JE01324.
Porter, C., Morin, P., Howat, I., Noh, M.-J., Bates, B., Peterman, K., Keesey, S., Schlenk, M., Gardiner, J., Tomko, K., Willis, M., Helleher, C., Cloutier, M., Husby, E., Foga, S., Nakamura, H., Platson, M., Wethington Jr., M., Williamson, C., Bauer, G., Enos, J., Arnold, G., Kramer, W., Becker, P., Doshi, A., D'Souza, C., Cummens, P., Laurier, F., Bojesen, M., 2018. ArcticDEM, Version 3. Harvard Dataverse, V1. https://doi.org/10.7910/DVN/C98DVS.
Price, S.F., Whillans, I.M., 2001. Crevasse patterns at the onset to Ice Stream B, West Antarctica. J. Glaciol. 47 (156). Retrieved from. https://www.cambridge.org/core.
Re, G.L., Fuller, I.C., Sofia, G., Tarolli, P., 2018. High-resolution mapping of Manawatu palaeochannels. N. Z. Geogr. 74 (2), 77–91. https://doi.org/10.1111/nzg.12186.
Rea, B.R., Evans, D.J.A., 2011. An assessment of surge-induced crevassing and the formation of crevasse squeeze ridges. J. Geophys. Res.: Earth Surf. 116 (F4) https://doi.org/10.1029/2011JF001970.
Ross, M., Campbell, J.E., Parent, M., Adams, R.S., 2009. Palaeo-ice streams and the subglacial landscape mosaic of the North American mid-continent prairies. Boreas 38, 421–439. https://doi.org/10.1111/j.1502-3885.2009.00082.x.
Sarif, M.N., Siddiqui, L., Islam, M.S., Parveen, N., Saha, M., 2021. Evolution of river course and morphometric features of the River Ganga: A case study of up and downstream of Farakka Barrage. Int. Soil and Water Conservation Research 9 (4), 578–590. https://doi.org/10.1016/j.iswcr.2021.01.006.
Sauramo, M., 1923. Studies on the Quaternary Varve Sediments in Southern Finland. In: Bulletin de la Commission Geologique de Finlande, 60. Suomen Geologinen Komissioni.
Scheidegger, A.E., 2002. Morphometric analysis and its relation to tectonics in Macaronesia. Geomorphology 46 (1–2), 95–115. https://doi.org/10.1016/S0169-555X(02)00056-9.
Schomacker, A., Benediktsson, I.O., Ingolfsson, O., 2014. The Eyjabakkajokull glacial landsystem, Iceland: Geomorphic impact of multiple surges. Geomorphology 218, 98–107. https://doi.org/10.1016/j.geomorph.2013.07.005.
Sharp, M., 1985. "Crevasse-Fill" Ridges: A Landform Type Characteristic of Surging Glaciers? Geogr. Ann. Phys. Geogr. 67 (3–4), 213–220. Retrieved from. https://www.jstor.org/stable/521009.
Simon, A., Castro, J., Rinaldi, M., 2016. Channel form and adjustment: characterization, measurement, interpretation and analysis. In: Mathias Kondolf, G., Piegay, Herve (Eds.), Tools in Fluvial Geomorphology, second ed. John Wiley & Sons, Ltd., Chichester, West Sussex https://doi.org/10.1002/9781118648551.ch11. 9780470684054.
Sinclair, S.N., Licciardi, J.M., Campbell, S.W., Madore, B.M., 2018. Character and origin of De Geer moraines in the Seacoast region of New Hampshire, USA. J. Quat. Sci. 33 (2), 225–237. https://doi.org/10.1002/jqs.3017.
Smith, G.W., 1982. End Moraines and the Pattern of Last Ice Retreat from Central and South Coastal Maine. Ohio University, Athens, Ohio, pp. 195–209.
Smith, M.J., Clark, C.D., 2005. Methods for the visualization of digital elevation models for landform mapping. Earth Surf. Process. Landforms 30, 885–900. https://doi.org/10.1002/esp.1210.
Smith, G.W., Hunter, L.E., 1989. Late Wisconsinan Deglaciation of Coastal Maine. In: Maine Geological Survey. Studies in Maine Geology, vol. 6. https://digitalmaine.com/cgi/viewcontent.cgi?referer=https://www.google.com/&httpsredir=1&article=1100&context=mgs_publications.
Soar, P.J., Wallerstein, N.P., Thorne, C.R., 2017. Quantifying River Channel Stability at the Basin Scale. Water 9 (2), 133. https://doi.org/10.3390/w9020133.
Sobota, I., Weckwerth, P., Nowak, M., 2016. Surge dynamics of Aavatsmarkbreen, Svalbard, inferred from the geomorphological record. Boreas 45, 360–376. https://doi.org/10.1111/bor.12160. ISSN: 0300-9483.
Solheim, A., 1991. The Depositional Environment of Surging Sub-Polar Tidewater Glaciers. A case study of the morphology, sedimentation and sediment properties in a surge-affected marine basin outside Nordaustlandet. Northern Barents Sea. Norsk Polarinstitutt, vol. 194, pp. 5-97. Oslo. Retrieved from. https://brage.npolar.no/npolar-xmlui/bitstream/handle/11250/173646/Skrifter194.pdf?sequence=1&isAllowed=y.
Sollid, J.L., 1989. Comments on the genesis of De Geer moraines. Norsk geografisk Tidsskrift - Norwegian Journal of Geography 43 (1), 45–47. https://doi.org/10.1080/00291958908552217. Oslo. ISSN: 0029-1951.
Stokes, C.R., 2000. The Geomorphology of Palaeo-Ice Streams: Identification, Characterisation and Implications for Ice Stream Functioning. The University of Sheffield. Retrieved from. https://core.ac.uk/download/pdf/77023352.pdf.
Stokes, C.R., 2018. Geomorphology under ice streams: Moving from form to process. Earth Surf. Process. Landforms 43, 85–123. https://doi.org/10.1002/esp.4259.
Stokes, C.R., Clark, C.D., 2001. Palaeo-ice streams. Quat. Sci. Rev. 20, 1437–1457. ISSN: 0277-3791. PII: S0277-3791(01)00003-8.
Storrar, R.D., Evans, D.J.A., Stokes, C.R., Ewertowski, M., 2015. Controls on the location, morphology and evolution of complex esker systems at decadal timescales, Breidamerkurjokull, southeast Iceland. Earth Surf. Process. Landforms 40, 1421–1438. https://doi.org/10.1002/esp.3725.
Stretch, R.C., Mitchell, N.C., Portaro, R.A., 2006. A morphometric analysis of the submarine volcanic ridge south-east of Pico Island, Azores. J. Volcanol. Geoth. Res. 156 (1–2), 35–54. https://doi.org/10.1016/j.jvolgeores.2006.03.009.

Streuff, K., Forwick, M., Szczucinski, W., Andreassen, K., Cofaigh, C.O., 2015. Submarine landform assemblages and sedimentary processes related to glacier surging in Kongsfjorden, Svalbard. Arktos 1 (14). https://doi.org/10.1007/s41063-015-0003-y.

Stromberg, B., 1965. Mappings and Geochronological Investigations in Some Moraine Areas of South-Central Sweden. Geogr. Ann. Phys. Geogr. 47 (2), 73–82, 10.1080.04353676.1965.11879715.

Székely, B., Karátson, D., 2004. DEM-based morphometry as a tool for reconstructing primary volcanic landforms: examples from the Börzsöny Mountains, Hungary. Geomorphology 63 (1–2), 25–37. https://doi.org/10.1016/j.geomorph.2004.03.008.

Valla, P.G., van der Beek, P.A., Lague, D., 2010. Fluvial incision into bedrock: Insights from morphometric analysis and numerical modeling of gorges incising glacial hanging valleys (Western Alps, France). JGR Earth Surface 115 (F2). https://doi.org/10.1029/2008JF001079.

Valters, D.A., 2016. Modelling Geomorphic Systems: Landscape Evolution. Geomorphological Techniques, Chap. 5, Sec. 6.12. British Society for Geomorphology. Retrieved from. https://www.geomorphology.org.uk/sites/default/files/chapters/5.6.12_LEM.pdf.

Virkkala, K., 1963. On Ice-Marginal Features in Southwestern Finland. In: Bulletin de la Commission Geologique de Finlande, 210. Geologinen Tutkimuslaitos, Helsinki.

Whillans, I.M., van der Veen, C.J., 2001. Transmission of stress between an ice stream and interstream ridge. J. Glaciol. 47 (158), 433–440. https://doi.org/10.3189/172756501781832052.

White, S.M., Haymon, R.M., Fornari, D.J., Perfit, M.R., Macdonald, K.C., 2002. Correlation between volcanic and tectonic segmentation of fast-spreading ridges: Evidence from volcanic structures and lava flow morphology on the East Pacific Rise at 9°-10°N. J. Geophys. Res. Solid Earth 107 (B8). https://doi.org/10.1029/2001JB000571. EPM 7-1-EPM 7-20.

Xie, Z., Huang, H., Yu, G., Zhang, M., 2018. Quantifying the Effects of Dramatic Changes in Runoff and Sediment on the Channel Morphology of a Large, Wandering River Using Remote Sensing Images. Water 10 (12), 1767. https://doi.org/10.3390/w10121767.

Zilliacus, H., 1989. Genesis of De Geer moraines in Finland. In: Sedimentary Geology, vol. 62. Elsevier Science Publishers B.V., Amsterdam - Printed in The Netherlands, pp. 309–317.